Modeling transient variations of permeability in coal seams at the reservoir scale

Najib Abouloifa, Matthieu Vandamme, Patrick Dangla

Modeling transient variations of permeability in coal seams at the reservoir scale

by N. Abouloifa, M. Vandamme[1], and P. Dangla
Navier, Ecole des Ponts, Univ Gustave Eiffel, CNRS, Marne-la-Vallée, France

Abstract

Production of fluid from or injection of fluid into a coal seam leads to variations of permeability of the seam, resulting from adsorption of fluid in the coal matrix in particular. One subtle effect is that, if the fluid pressure in the cleat increases, after an immediate opening of the cleat, one expects the cleat aperture (and hence the permeability) to decrease for a transient time, as a consequence of the fluid diffusion from the cleat to the coal matrix. In this work, we aim to model such transient variations of permeability by proposing constitutive equations at the fractured coal scale. Permeability depends on the complete history of pressures over time. The constitutive equations rely on Boltzmann's superposition principle, which requires kernels as inputs. One can identify the kernels with finite-element simulations of the response of an individual cleat subjected to a history of fluid pressure. We also propose approximate versions of those kernels, which only depend on a few parameters with a physical meaning. Examples of fluid injection simulations into a coal seam making use of the constitutive equations here derived are presented.

1 Introduction

Unminable coal seams could contribute to the storage of CO_2 (i.e., carbon dioxide) up to 20 Gt (Gale, 2004). Given that anthropogenic emissions of CO_2 are estimated at 10 Gt per year (Knorr, 2009), coal seams could contribute to store about two years of those emissions, which is small but non-negligible. Unminable coal seams contain CH_4 (i.e., methane) naturally: proven resources are 2 billion standard cubic feet, and contingent resources are estimated at 300 billion standard cubic feet (Moore, 2012). Natural gas presently contributes to about 21% of the world's energy supply (International Energy Agency, 2019). Production of CH_4 can be enhanced by injecting CO_2 into the seam –a process known as CO_2-enhanced coal bed methane recovery (or CO_2-ECBM). During both injection of CO_2 (Oudinot et al., 2011; Pekot and Reeves, 2002) and production of CH_4 (Palmer and Mansoori, 1998; Moore et al., 2011; Scott et al., 2012), significant variations of permeability are observed. The reason beyond those variations is well known: they are the consequence of adsorption-induced volume variations of the coal (Gray, 1987).

Naturally, coal is a fractured material (Laubach et al., 1998): those natural fractures are called cleats, vary in size, are mostly vertical, and are spaced by about a centimeter. Cleats govern the seam's permeability (Mazumder et al., 2006; Pan and Connell, 2007). Between cleats, one finds the coal matrix (Harpalani and Schraufnagel, 1990), porous, with pores down to a sub-nanometric size. The variations of permeability observed during production or injection are due to the cleats' opening or closure, which is consecutive to shrinkage or swelling of the coal matrix, respectively. Dimensional variations of the coal matrix observed upon variations of the pressure of the fluid it contains are known to be due to adsorption

[1] Corresponding author

effects (Levine, 1996). In the smallest pores of the material, most of the fluid it contains is indeed adsorbed, i.e., in intermolecular interaction with the solid skeleton's atoms. Because of those intermolecular interactions, an unconstrained piece of coal matrix tends to swell upon an increase of fluid pressure. The magnitude of those pressure-induced dimensional variations depends on the fluid. Upon CO_2 injection, the injection induces increased CO_2 pressure in the bed and coal matrix swelling. In the confined conditions that prevail in the underground, this swelling translates into cleats closure, and finally into permeability decrease.

Subtle adsorption-induced variations of permeability can take place. Let us consider a sample of fractured coal submitted to constant confining stresses, in which we inject fluid. Because the cleat system's permeability is larger than that of the coal matrix, fluid will first penetrate the cleats (such flow of fluid or transfer of mass through the cleats is also referred to as seepage (Barenblatt et al., 1960)). It will decrease the effective stress, hence leading to an aperture of the cleats and increasing the sample's permeability. Immediately after the injection, fluid will start penetrating the coal matrix through Fickian diffusion (Moore, 2012). At early times, the concentration of fluid in the coal matrix must be larger in the vicinity of the cleat than far from it (see Figure 1-b). Even if the sample is under constant confining stresses, the coal matrix's swelling will be localized around the cleat, which will tend to close the cleat. At large times, the concentration of fluid in the coal matrix should be homogeneous. In this case, if the sample is under constant confining stresses and the coal matrix is homogeneous, swelling of the coal matrix should translate into a homothetic swelling of the whole sample and hence of the cleats as well, leading to a long-term increase of permeability (see Figure 1-a at large times). As a result, even if fluid pressure in the cleats is constant over time, one can expect a non-monotonic and complex variation of permeability, as displayed in Figure 1-a. This complex variation results from the transient diffusion of fluid through the coal matrix and the induced heterogeneity of fluid pressure in the matrix. We will refer to those variations as “transient variations of permeability.”

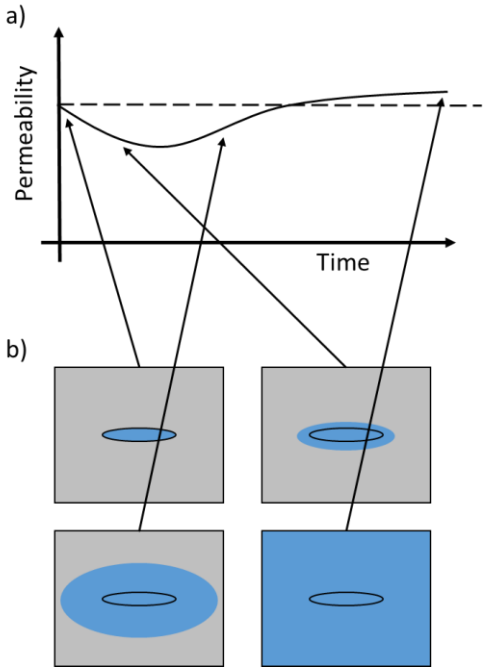

Figure 1: Schematics of (a) transient variations of permeability and (b) distribution of fluid in the coal. The black ellipse represents the cleat, and we display the injected fluid in blue. The dashed line on subfigure (a) indicates the initial permeability.

The study of those transient variations of permeability has gained significant interest recently. With finite-element simulations of coal samples (Peng et al., 2014b; Qu et al., 2014; X. Liu et al., 2018) or through review of laboratory data (Liu et al., 2011a), several studies showed that the diffusion of fluid through the coal matrix could yield non-monotonic variations of permeability of significant magnitude. Assuming local thermodynamic equilibrium (i.e., assuming that, inside a representative elementary volume of fractured coal, the fluid's thermodynamic pressure is homogeneous, i.e., the same at any location in the coal matrix as in the cleats) can yield significant errors.

On laboratory samples submitted to constant confining stresses, several groups (Robertson, 2005; Pini et al., 2009; Wang et al., 2011) observed non-monotonic variations of permeability with the pore fluid's pressure –a phenomenon known as permeability rebound. Liu et al. (2011b), Peng et al. (2014a), and Qu et al. (2014) proposed to explain this permeability rebound by the fact that experimental data would have been acquired before reaching an equilibrium or a steady-state. Therefore, this permeability rebound would be a consequence of transient variations of permeability. Experimentally, Wei et al. (2019b) observed non-monotonic evolutions of permeability with time for a coal sample submitted to constant confining stresses and fluid pressures, which, according to them, suggests a transition from a swelling nearby the cleat to further away. Note, however, that other theories can explain the permeability rebound without invoking transient effects. For instance, by assuming that a fraction of the bulk coal swelling or of the matrix coal swelling translates into the closure of the cleats, models can capture permeability rebound. This ability holds independent of whether the fraction is considered constant (Liu and Rutqvist, 2010; Connell et al., 2010; Chen et al., 2012; Guo et al., 2014; Lu et al., 2016; Z. Liu et al., 2018) or pressure-

dependent (Peng et al., 2017). Heterogeneity of coal (Izadi et al., 2011; Chen et al., 2013), as well as gas slippage (Niu et al., 2018) or a transition between different flow regimes (Wang et al., 2019) could also explain complex variations of the permeability with pore pressure for a piece of coal submitted to constant confining stresses.

Our aim in this work is to model transient variations of permeability in reservoir simulations. As Peng et al. (2014b), Qu et al. (2014), and X. Liu et al. (2018) showed, those transient variations of permeability can be modeled numerically as soon as the coal matrix around the cleat is meshed and the diffusion of fluid through the coal matrix is explicitly modeled. However, such an approach cannot be employed to perform reservoir simulations, as the number of elements required to perform such simulation would be much too large. Consequently, we aim at deriving a model at a scale such that the representative elementary volume is a piece of fractured coal.

At our scale of interest, i.e., at the scale where a piece of fractured coal is our representative elementary volume (seen as a smeared porous medium), many have modeled adsorption-induced variations of permeability (for a review, see Pan and Connell (2012)). Most models (e.g., Palmer and Mansoori (1998), Shi and Durucan (2004), Cui and Bustin (2005), Vandamme et al. (2010), Pijaudier-Cabot et al. (2011), Wu et al. (2011), Brochard et al. (2012), Espinoza et al. (2014)) assume local thermodynamic equilibrium. This assumption means that, by nature, those models are unable to capture the non-monotonic variations of permeability displayed in Figure 1-a, as those variations are the direct consequence of the heterogeneity of the concentration of fluid in the coal matrix within the representative elementary volume. In contrast, others aimed at relaxing this assumption of local thermodynamic equilibrium (Wu et al., 2010; Liu et al., 2011b; Wu et al., 2011; Peng et al., 2014a; Vandamme et al., 2014; Zang and Wang, 2017; Wei et al., 2019a).

Barenblatt et al. (1960) modeled fluid flow in fractured rocks by introducing variables averaged over a scale much larger than the spacing between fractures. They considered two pressures of fluid at each point in space, i.e., one in the fractures and one in the pore space in the rock between the fractures. They considered the transfer of fluid between fractures and rock porosity, but, by construction, in their model, the fluid pressure is homogeneous in the whole rock porosity at each point in space. In the same spirit, but specifically for coal, Wu et al. (2010, 2011) and Vandamme et al. (2014) introduced kinetics of transfer between cleats and coal matrix. But they considered that the thermodynamic pressure of fluid in the coal matrix is homogeneous: such simplification makes it impossible to capture the non-monotonic variations of permeability displayed in Figure 1-a. To solve this issue, the model of Liu et al. (2011b) and its extension to double-porosity media (Peng et al., 2014a) introduce the notion of local and global swelling. In fact, in those models, in a representative elementary volume of fractured coal, one pressure of the fluid in the cleats and one pressure of the fluid in the coal matrix is defined, which can differ. But fluid in the cleats is considered to make the cleat's vicinity swell so that the cleats aperture (and thus the permeability) decreases with increased fluid pressure in the cleat. Upon fluid injection in an unconfined sample, both the fluid pressure in the cleats and the coal matrix vary. After an immediate opening of the cleats, the cleats' fluid pressure tends to close the cleats in the short term. In unconfined conditions, the fluid pressure in the matrix tends to open the cleats in the long term. Those two kinetics compete. Zang and Wang (2017) also relax the local thermodynamic equilibrium condition by introducing a non-equilibrium swelling and defining the kinetics that governs this non-

equilibrium swelling related to fluid diffusion in the coal matrix. Like the model of Liu et al. (2011b), this model can capture non-monotonic evolutions of permeability upon injection into an unconfined piece of coal, depending on the kinetics of increase of fluid pressure in the cleats and the coal matrix. Wei et al. (2019a) consider that the transient variation of the cleats' aperture is related to the gradient of fluid pressure in the coal matrix. Therefore, they postulate that it is associated with the rate of coal matrix swelling. By doing so, they end up with a model able to capture non-monotonic transient variations of permeability.

In this work, we aim to propose constitutive equations that can model transient permeability variations in reservoir simulations. Hence, we formulate them at a scale such that the representative elementary volume is a small piece of fractured coal. Our approach is original and alternative to the previous paragraph's models, as it relies on the Boltzmann superposition principle. In such a framework, we can model the transient variations of permeability predicted by simulations of fluid injection in an individual cleat with constitutive equations formulated at a scale above (i.e., at a scale at which the representative elementary volume contains both coal matrix and cleats). The fact that this upscaling is exact represents the main interest of the model we propose.

Section 2 starts by performing finite-element simulations of fluid injection in a cleat surrounded by the coal matrix. Those simulations, performed at a scale lower than the one at which we aim at deriving our model, make it possible to understand the process at stake better and serve as a reference case. This section also presents the principle of the modeling proposed, which relies on the Boltzmann superposition principle. In section 3, we derive the constitutive equations able to capture transient variations of permeability at the scale of a representative elementary volume of fractured coal. We also implement those equations and simulate fluid injection into a reservoir by using the results of the finite-element simulations performed in section 2 as input. In section 4, we propose an engineering version of our model, with which we can model transient variations of permeability by introducing just a few parameters with a physical meaning.

2 Transient variations of permeability of an individual cleat whose permeability is governed by its aperture

This section considers a system made of a single cleat surrounded by an isotropic coal matrix. The cleat is cylindrical and infinitely long. The history of pressure $p_c(t)$ of the fluid in the cleats is imposed and is homogeneous in the cleat. Consequently, the problem is 2-dimensional, and we focus on what happens in a slice perpendicular to the direction of the cleat (i.e., in the plane visible in Figure 1-b). We aim to simulate numerically (see section 2.2) and then model (see section 2.3) how this system reacts to the history of pressure, particularly in terms of permeability and transfer of fluid from the cleat to the coal matrix.

We give the various geometries of cleats considered in this study in Figure 2. All cleats are embedded in a square with edges with a length equal to 1 cm. We consider one cleat with a rectangular cross-section (called `rectangular cleat') of dimensions 0.05 cm by 0.5 cm. We also consider cleats with an elliptical cross-section (called `elliptical cleats') of a long axis $A = 0.25$ cm and of short axis a. Various ratios a/A are considered: 0.03, 0.10, 0.30, 1.00. The cleat with aspect ratio $a/A = 1$ corresponds to a cleat with a circular cross-section.

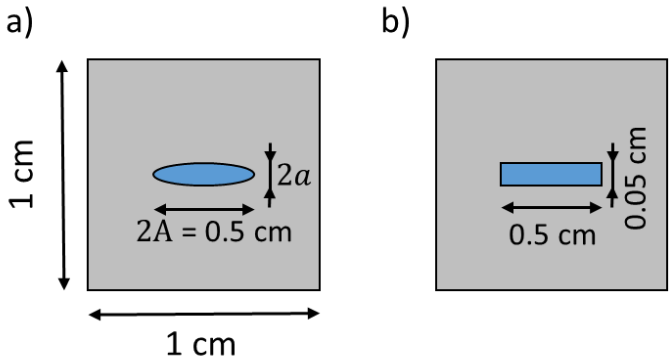

Figure 2: Various geometries of the cross-section of cleats considered in this study: cleats with (a) an elliptical cross-section and (b) a rectangular cross-section.

The intrinsic permeability $\kappa(t)$ of the cleat is assumed to be governed by its aperture and to follow the celebrated Kozeny-Carman relationship (Coussy, 2010):

$$\kappa \propto \frac{(\phi_c)^3}{(1-\phi_c)^2}, \tag{1}$$

where ϕ_c is the porosity associated with the cleat system and is defined as:

$$\phi_c = \frac{V_c}{V_0} \tag{2}$$

where V_c is the actual volume of cleats in the volume of fractured coal of interest. In the reference configuration, the volume of fractured coal of interest is V_0. Under the assumption that the porosity is much smaller than 1, Eq. (1) reduces to:

$$\kappa = \kappa_0 \left(\frac{V_c}{V_{c,0}}\right)^3 = \kappa_0 \left(1 + \frac{\Delta V_c}{V_{c,0}}\right)^3 \tag{3}$$

where κ_0 is the permeability in the reference configuration, $V_{c,0}$ is the volume of the cleats in the reference configuration, and ΔV_c is the variation of the volume of the cleats.

2.1 Equations governing the problem

We consider that the cleat is subjected to a fluid pressure $p_c(t)$. At a given time t, the thermodynamic pressure $p_m(y,z,t)$ of the fluid in the coal matrix (where y and z are coordinates in the plane of interest) is, in the generic case, heterogeneous.

The Langmuir adsorption isotherm relates the mass concentration $c_m(y,z,t)$ of fluid in the coal matrix (per unit volume of coal matrix in the reference configuration) to the thermodynamic pressure $p_m(y,z,t)$ of the fluid in the coal matrix through:

$$c_m(y,z,t) = c_{m,max} \frac{p_m(y,z,t)/p_{L0}}{1 + p_m(y,z,t)/p_{L0}} \tag{4}$$

where $c_{m,max}$ and p_{L0} are Langmuir parameters.

The pressure $p_c(t)$ of fluid in the cleats imposes the thermodynamic pressure $p_m(y,z,t)$ of fluid on the edge of the cleat and hence the concentration $c_{edge}(t)$ of fluid in the coal matrix on the edge of the cleat, through:

$$c_{edge}(p_c(t)) = c_{m,max}\frac{p_c(t)/p_{L0}}{1+p_c(t)/p_{L0}} \quad (5)$$

The transport of fluid in the coal matrix is assumed to be diffusive and to follow Fick's law (Moore, 2012) so that the mass flow vector $\underline{w_m}$ of fluid through the coal matrix verifies:

$$\underline{w_m} = -D\underline{\nabla c_m} \quad (6)$$

where D is the diffusivity of the fluid through the coal matrix. For engineering applications, it is common to consider that the diffusivity D is constant (which we will assume here), while in practice, it may not be (Zhao et al., 2019). The mass concentration of fluid then verifies:

$$\frac{\partial c_m}{\partial t} = D\Delta c_m \quad (7)$$

The coal matrix is assumed to behave in a linear elastic manner. We note its stiffness tensor $\boldsymbol{C_m}$. Its bulk modulus is K_m and its Poisson's ratio ν_m. Adsorption roughly makes a piece of coal swell proportionally to the concentration c_m of fluid in the coal matrix, so that the constitutive equation of the coal matrix is:

$$\underline{\underline{\sigma}} = \boldsymbol{C_m}\colon\left(\underline{\underline{\varepsilon}} - \varepsilon^a(c_m)\underline{\underline{1}}\right) \text{ with } \varepsilon^a(c_m) = \alpha c_m \quad (8)$$

where ε^a is an adsorption strain and α a parameter governing the magnitude of adsorption-induced swelling. Likewise, we can express this equation as:

$$\underline{\underline{\sigma}} = \boldsymbol{C_m}\colon\underline{\underline{\varepsilon}} + \sigma^a(c_m)\underline{\underline{1}} \text{ with } \sigma^a(c_m) = -3K_m\varepsilon^a(c_m) = -3K_m\alpha c_m \quad (9)$$

where we call $\sigma^a(c_m)$ adsorption stress.

2.2 Numerical solution of response to a step loading

We perform two-dimensional simulations with Abaqus. We use plane-strain conditions and consider no confining stress, i.e., $\sigma_0 = 0$. Note that, by considering non-zero constant confining stress, we would have calculated identical variations of aperture. We give properties and conditions in Table 1. We obtained material properties in this table from the literature. The maximum adsorbed amount $c_{m,max}$ expressed in kg.m^{-3} is calculated from the maximum adsorbed amount of $2.4\ \text{mol.L}^{-1}$ in Espinoza et al. (2014) as: $c_{m,max} = (2.4\ \text{mol.L}^{-1}) * M_{CO_2}$ where $M_{CO_2} = 44\ \text{g/mol}^{-1}$ is the molar mass of CO_2. The parameter α expressed in m^3.kg^{-1} is calculated from the swelling coefficient $4 * 10^{-3}\ \text{L.mol}^{-1}$ in Espinoza et al. (2014) as $\alpha = 4 * 10^{-3}\ \text{L.mol}^{-1}/M_{CO_2}$.

Table 1: Input parameters for computation

Parameter	Value	Reference
Diffusivity $\boldsymbol{D}$ of fluid in coal matrix ($m^2.s^{-1}$)	$1.0 \cdot 10^{-9}$	Order of magnitude from Nazarova et al. (2014)
Bulk modulus $\boldsymbol{K_m}$ of coal matrix (GPa)	5.0	(Espinoza et al., 2014)
Poisson's ratio $\boldsymbol{\nu_m}$ of coal matrix (1)	0.2	Order of magnitude from Espinoza et al. (2014)
Maximum adsorbed amount $\boldsymbol{c_{m,max}}$ in Langmuir isotherm ($kg.m^{-3}$)	105.6	Calculated from Espinoza et al. (2014)
Characteristic pressure $\boldsymbol{p_{L0}}$ in Langmuir isotherm (MPa)	1.6	Espinoza et al. (2014)
Parameter $\boldsymbol{\alpha = \Delta\varepsilon^a/\Delta c_m}$ governing the magnitude of adsorption-induced swelling ($m^3.kg^{-1}$)	$9.1 \cdot 10^{-5}$	Calculated from Espinoza et al. (2014)
Temperature T (°C)	40	
Confining stress $\boldsymbol{\sigma_0}$ (MPa)	0	

We apply a step loading of fluid pressure in the cleat:

$$p_c(t) = \begin{cases} 0 & \text{if } t \leq 0 \\ p_{c,0} & \text{if } t > 0 \end{cases} \quad (10)$$

Consequently, the hydric boundary conditions on the edge $\partial\Omega_{in}$ of the cleat are:

$$c_m(y,z,t) = c_{edge}(t) = \begin{cases} 0 & \text{if } t \leq 0 \\ c_{m,max}\dfrac{p_{c,0}/p_{L0}}{1 + p_{c,0}/p_{L0}} & \text{if } t > 0 \end{cases} \quad (11)$$

On all boundaries other than the edge of the cleat, we impose no flux.

The mechanical boundary conditions on the edge $\partial\Omega_{in}$ of the cleat are:

$$\underline{\underline{\sigma}}.\underline{n} = \begin{cases} 0 & \text{if } t \leq 0 \\ -p_c\underline{n} & \text{if } t > 0 \end{cases} \quad (12)$$

As stated in Table 1, on the outer boundaries, we impose no stress. On the boundaries that correspond to planes of symmetry of the modeled system, we impose mechanical boundary conditions that are consistent with the symmetry, namely free sliding parallel to the boundary and no displacement perpendicular to the boundary.

We give an example of the distribution of concentration around a cleat with an elliptical cross-section in Figure 3.

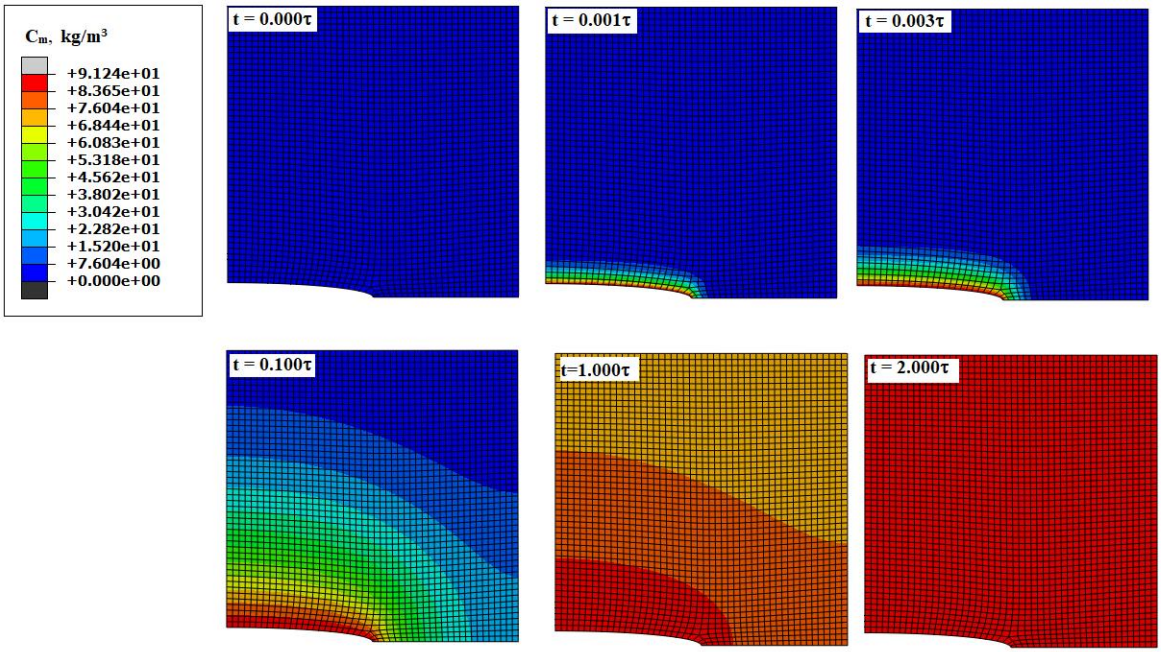

Figure 3: Distribution of fluid concentration c_m in the coal matrix at various times around a cleat with an elliptical cross-section and an aspect ratio $a/A = 0.03$.

The variation ΔV_c of the cleat's volume is calculated from the displacements $\underline{\xi}$ of the edges of the cleat according to:

$$\Delta V_c = -\int_{\partial\Omega_{in}} \underline{\xi}.\underline{n}\, dS \qquad (13)$$

where $\underline{n}$ is the vector normal to the inner surface $\partial\Omega_{in}$ of the region occupied by the coal matrix. For some of the geometries considered, normalized variations $\Delta V_c/V_{c,0}$ of the aperture of the cleat are displayed in Figure 4. From those variations of aperture, variations of permeability can be readily obtained with the Kozeny-Carman equation (3), as displayed in Figure 5.

On those figures, one observes that, for cleats with a circular cross-section, permeability increases monotonically with time. For all other cleats with a cross-section with an aspect ratio different from 1.0, permeability varies in a nonmonotonic manner, first decreasing at early times before increasing at larger times. In all cases, permeability at equilibrium is larger than permeability at early times since, in unconfined conditions, the coal matrix's swelling translates into a homothetic swelling of the sample and hence of the cleat as well.

For a given aspect ratio, the geometry of the cross-section (namely elliptical (see Figure 4-b and Figure 5-b) or rectangular (see Figure 4-d and Figure 5-d)) impacts the evolutions of permeability over time, but not very significantly. However, we note that, for given fluid pressure, the immediate increase of permeability is larger for the cleat with a rectangular cross-section (see Figure 4-d) than with an elliptical one (see Figure 4-b). For cleats with an elliptical cross-section, when the aspect ratio decreases (i.e., when the cleat is flatter), both the transient reduction of permeability and the immediate increase of permeability (i.e., the poroelastic effect due to the mechanical pressure of the fluid on the pore walls) are more pronounced. In contrast, the characteristic time to reach equilibrium seems roughly

independent of the cleat's cross-section geometry. The time at which permeability is the lowest is equal to about 1500s for the cleat with a rectangular cross-section whose aspect ratio is 0.3 and for cleats with an elliptical cross-section whose aspect ratio is 0.1 or 0.03. This time is equal to about 750s for the cleat with an elliptical cross-section whose aspect ratio is 0.3. For sufficiently flat cleats, the time at which permeability is the lowest is roughly independent of the cleat's cross-section geometry. We will discuss those trends further in a quantitative analysis of the time-dependent response performed in Section 4.2.

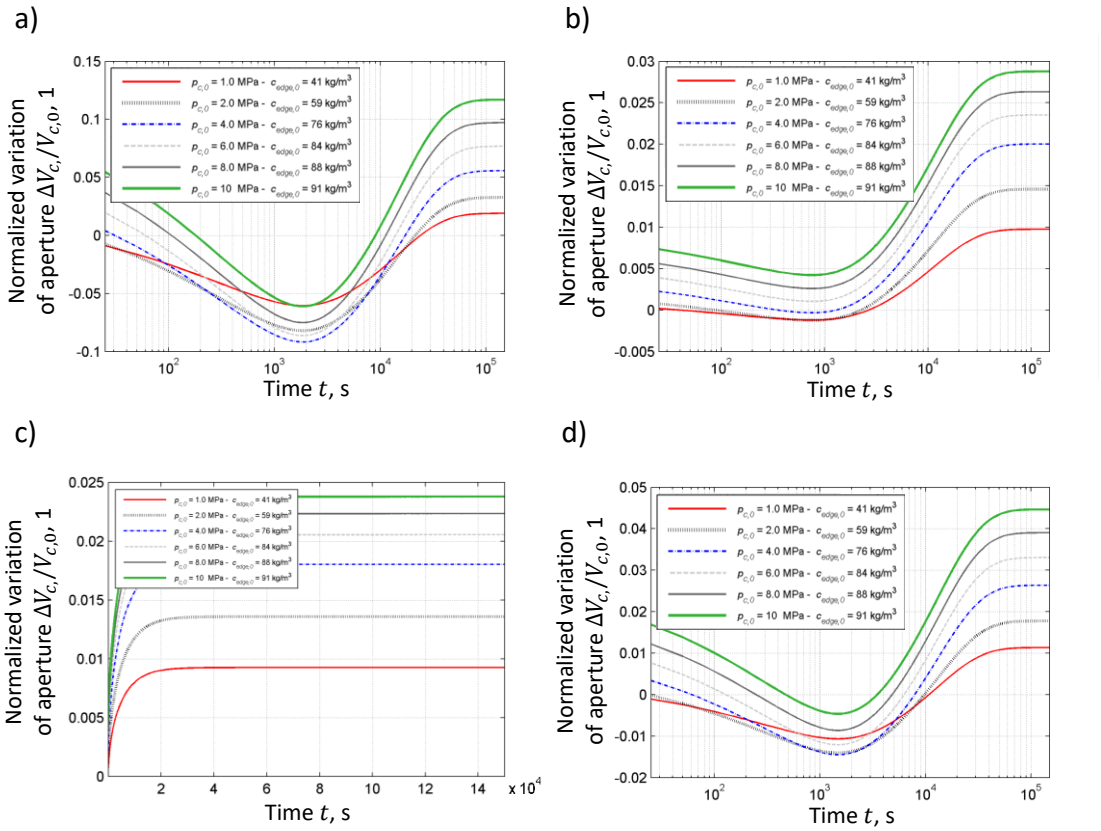

Figure 4: Evolution over time of cleat aperture for cleats with various geometries subjected to various fluid pressures: (a) elliptical cross-section with aspect ratio $a/A = 0.03$, (b) elliptical cross-section with aspect ratio $a/A = 0.3$, (c) elliptical cross-section with aspect ratio $a/A = 1.0$, (d) rectangular cross-section with aspect ratio $a/A = 0.3$.

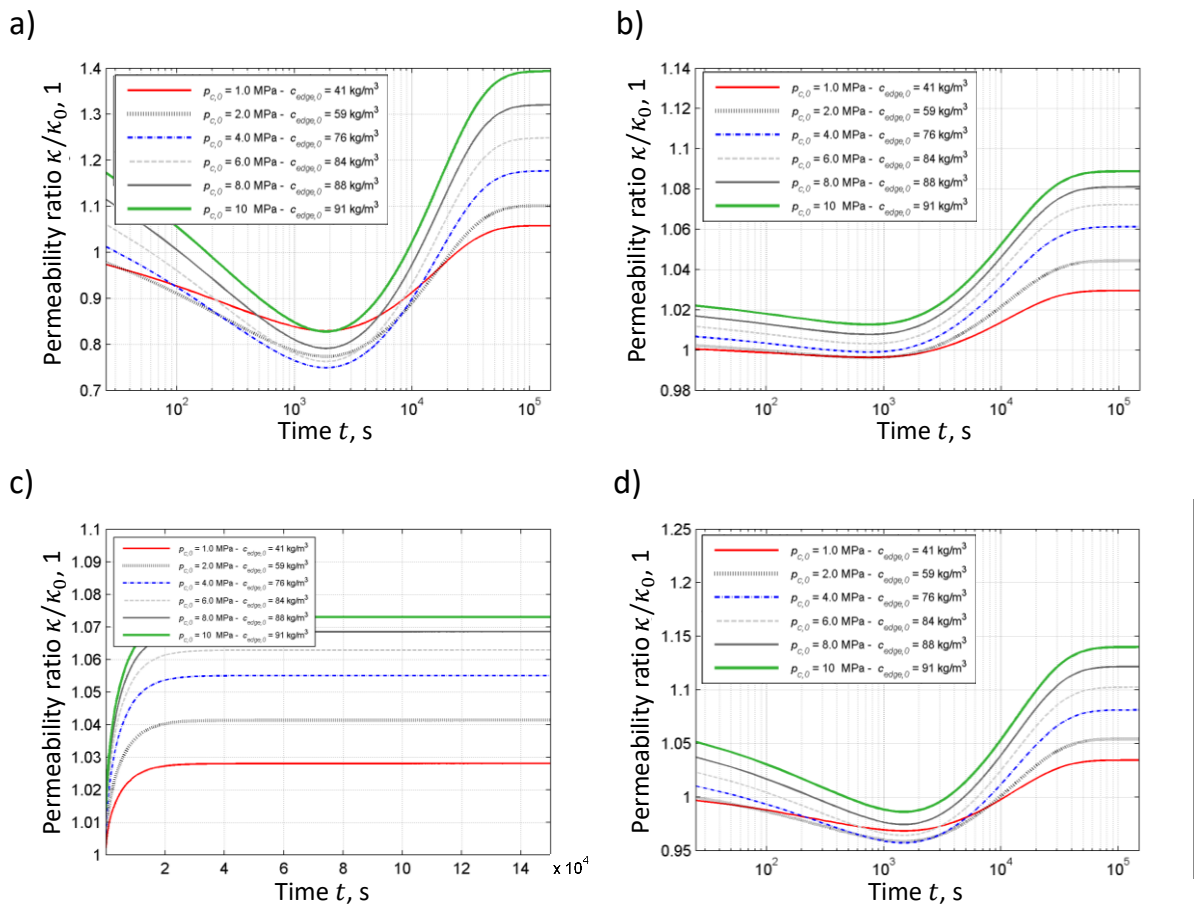

Figure 5: Evolution over time of permeability for cleats with various geometries subjected to various fluid pressures: (a) elliptical cross-section with aspect ratio $a/A = 0.03$, (b) elliptical cross-section with aspect ratio $a/A = 0.3$, (c) elliptical cross-section with aspect ratio $a/A = 1.0$, (d) rectangular cross-section with aspect ratio $a/A = 0.3$.

From the simulations performed, the flow rate dm_m/dt of fluid from the cleats to the coal matrix (expressed per unit volume V_0 of fractured coal in the reference configuration) can be calculated by spatial integration of the flux on the edges of the cleat:

$$\frac{dm_m}{dt} = -\frac{1}{V_0}\int_{\partial\Omega_{in}} \underline{w_m}.\underline{n}dS \qquad (14)$$

The amount m_m of fluid in the coal matrix (still per unit volume V_0 of fractured coal in the reference configuration) can be calculated by integration over time of Eq. (14).

The average mass $< c_m >$ of fluid in the coal matrix per unit volume of coal matrix in the reference configuration is displayed in Figure 6 for the example of the elliptical cleat with an aspect ratio $a/A = 0.03$. In this figure, time is displayed in a dimensionless manner by dividing it by a characteristic time $\tau = 25{,}000$ s, which corresponds to $\tau = {L_{diff}}^2/D$, where $D = 1 \times 10^{-9}$ m²/s is the diffusion coefficient of the coal matrix and $L_{diff} = 0.5$ cm is a drainage length equal to half of the characteristic spacing between cleats. The value toward which $< c_m(t) >$ should converge at large times is known: it should tend toward $c_{edge,0}$, since the concentration of fluid in the coal matrix per unit of coal matrix should be homogeneous and equal to its value $c_{edge,0}$ on the edge of the cleat. We noticed however a slight

discrepancy, as $< c_m(t) >$ tended toward values that slightly differed from the expected one. We attributed this discrepancy to numerical errors. In the rest of the manuscript, we rescaled all values of $c_m(t)$ (and consequently of $m_m(t) = (1 - \phi_{c,0})c_m(t)$ and of $\dot{m}_m$) based on the calculated asymptotic value of $c_m(t)$, to ensure that the rescaled $c_m(t)$ properly converged toward the expected value $c_{edge,0}$. Hence, the rescaled $m_m(t)$ also properly converges toward its expected valued, namely $(1 - \phi_{c,0})c_{edge,0}$.

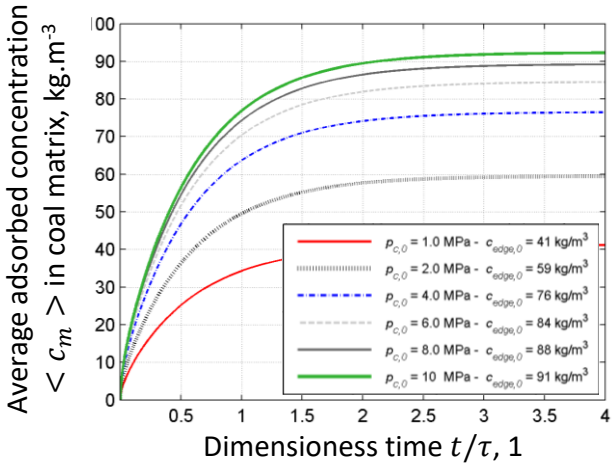

Figure 6: Evolution of average mass $< c_m(t) >$ of fluid in coal matrix per unit volume of coal matrix, for the elliptical cleat with an aspect ratio $a/A = 0.03$. The characteristic time τ used to make the time dimensionless is $\tau = 25{,}000$ s.

2.3 Principle of the solution to a generic loading: analogy with linear viscoelasticity

This section is devoted to explaining how, based on the cleat's response to a step loading of fluid pressure simulated in section 2.2, we can calculate the cleat's response to a generic fluid pressure evolution. The approach is based on the Boltzmann superposition principle.

Part of the variation ΔV_c of the cleat's volume is due to the deformation induced by the fluid's mechanical pressure on the cleat's walls and by the confining stress potentially applied to the system, while another part of the variation is due to the diffusion of fluid in the coal matrix and to the swelling it induces, i.e.:

$$\Delta V_c = \Delta V_{c,mech} + \Delta V_{c,hydr} \qquad (15)$$

where $\Delta V_{c,mech}$ is the contribution due to the mechanical loading (called `mechanical contribution') and $\Delta V_{c,hydr}$ is the contribution due to the diffusion of fluid in the coal matrix (called `hydraulic contribution'). For the case of the elliptical cleat with an aspect ratio $a/A = 0.03$, we display the two contributions in Figure 7.

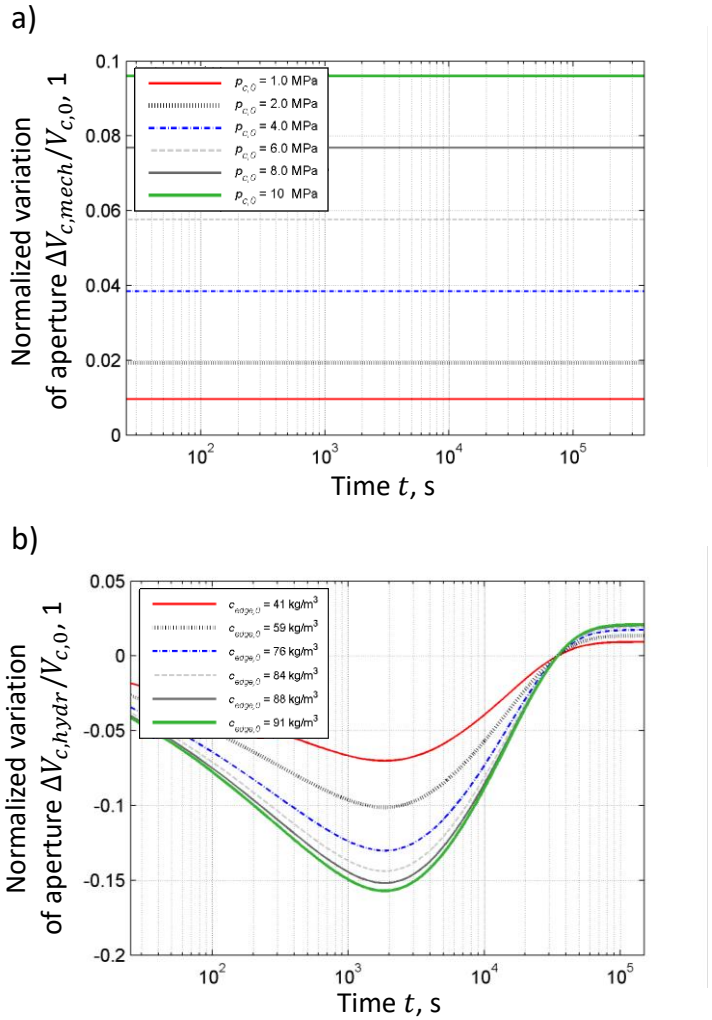

Figure 7: For an elliptical cleat with aspect ratio $a/A = 0.03$, mechanical contribution $\Delta V_{c,mech}$ and hydraulic contribution $\Delta V_{c,hydr}$ to the variation ΔV_c of the volume of the cleat.

The mechanical contribution $\Delta V_{c,mech}$ to the variation ΔV_c of the cleat's volume depends linearly on the pressure $p_c(t)$ of the fluid in the cleats and on the confining stress $\sigma_0(t)$:

$$\frac{\Delta V_{c,mech}(t)}{V_{c,0}} = \frac{p_c(t)}{K_{c,p}} + \frac{\sigma_0(t)}{K_{c,\sigma}} \qquad (16)$$

where $K_{c,p}$ and $K_{c,\sigma}$ characterize the stiffness of the cleat. Since we performed the calculations in section 2.2 in the absence of any confining stress (i.e., $\sigma_0 = 0$), we restrict ourselves to the case where the variation $\Delta V_{c,mech}/V_{c,0}$ is proportional to the fluid pressure $p_c(t)$:

$$\frac{\Delta V_{c,mech}(t)}{V_{c,0}} = \frac{p_c(t)}{K_{c,p}} \qquad (17)$$

In contrast, even in the case of a step of fluid pressure (i.e., $p_c(t) = p_{c,0}$), the hydraulic contribution $\Delta V_{c,hydr}(t)$ at any time t is not proportional to the pressure $p_{c,0}$ of fluid in the cleats, as can be observed in Figure 8-a in the case of the elliptical cleat with aspect ratio $a/A = 0.03$. But transport of fluid is a linear process (see Eq. (7)), and swelling depends linearly on the concentration $c_{edge,0}$ on the edge of the cleat as well (see Eqs. (8) and (9)), so that the hydraulic contribution $\Delta V_{c,hydr}(t)$ at any time t is proportional to this concentration,

as can be observed in Figure 8-b. If we consider this concentration $c_{edge,0}$ on the edge of the cleat as the variable with which to formulate the problem, we can hence consider coal as a Boltzmann-type material, for which the superposition of the action implies the superposition of the responses, and for which one can express the evolution of the aperture of the cleat as follows:

$$\frac{\Delta V_{c,hydr}}{V_{c,0}} = \begin{cases} J_{\delta_c}(t).\, c_{edge,0} \text{ if } t > 0 \\ 0 \text{ if } t \leq 0 \end{cases} \quad (18)$$

Here we call $J_{\delta_c}(t)$ the kernel of the variation of aperture due to the ingress of fluid in the coal matrix. It is the response to a unit step of concentration $c_{edge,0} = 1$ kg/m^3.

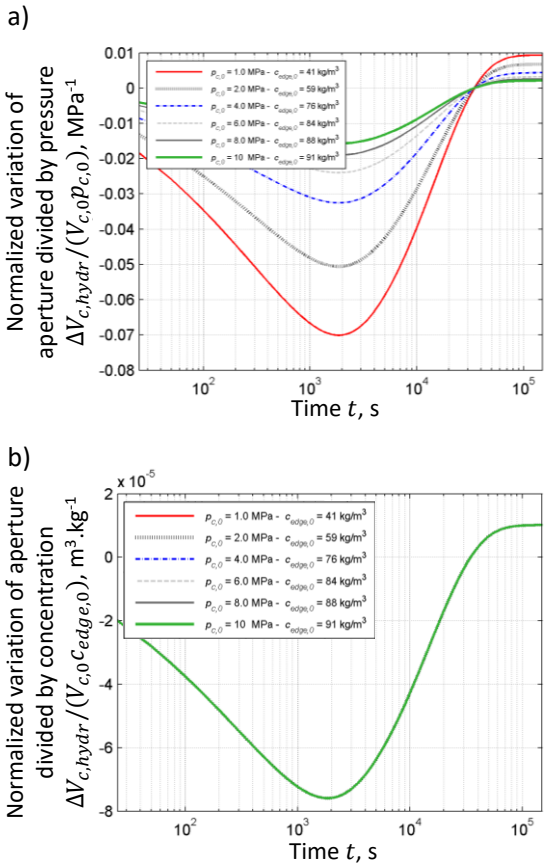

Figure 8: For elliptical cleat with aspect ratio $a/A = 0.03$, contribution of the fluid in the matrix to the variation of aperture (a) normalized by the pressure of the fluid in the cleat or (b) normalized by the concentration on the edge of the cleat.

Let us now consider a generic injection of fluid following a history of pressure $p_c(t)$ in the cleat. This injection causes a history of concentration $c_{edge}(t)$ on the edge of the cleat (see Eq. (5)). We consider that this function $c_{edge}(t)$ is piecewise continuous and differentiable. We note τ_i the instances where c_{edge} is discontinuous and $[c_{edge}]_i$ the corresponding jumps of the concentration on the edge of the cleat. Therefore, the concentration function $c_{edge}(t)$ can be rewritten as:

$$c_{edge}(t) = \int_{-\infty}^{t} Y(t-\tau) dc_{edge} + \sum_{\tau_i<t} \left[c_{edge}\right]_i Y(t-\tau_i) \quad (19)$$

where $Y(t)$ is the Heaviside function. The response $\Delta V_{c,hydr}(t)$ of the cleat aperture to the variations of concentration is derived directly from the application of Boltzmann superposition principle to Eq. (19):

$$\frac{\Delta V_{c,hydr}}{V_{c,0}} = \int_{-\infty}^{t} J_{\delta_c}(t-\tau) dc_{edge} + \sum_{\tau_i<t} \left[c_{edge}\right]_i J_{\delta_c}(t-\tau_i) \quad (20)$$

We can write Eq. (20) by using Stieltjes integrals as follows:

$$\frac{\Delta V_{c,hydr}}{V_{c,0}} = J_{\delta_c}(t) \otimes c_{edge}(t) = \int_{\tau=-\infty}^{t} J_{\delta_c}(t-\tau) \frac{\partial c_{edge}}{\partial \tau}(\tau) d\tau \quad (21)$$

with:

$$\frac{\partial c_{edge}}{\partial t} = \left\{\frac{\partial c_{edge}}{\partial t}\right\} + \sum_{\tau_i<t} \left[c_{edge}\right]_i \delta(t-\tau_i) \quad (22)$$

where $\delta(t)$ is the Dirac function, {} is the derivative of the continuous part of the concentration $c_{edge}(t)$, and where $\otimes$ denotes the Stieltjes convolution product.

Combining Eqs. (3), (15), (16), and (21), we can finally express the variation of permeability for a generic loading:

$$\begin{aligned} \kappa(t) &= \kappa_0 \left(1 + \frac{\Delta V_{c,mech}}{V_{c_0}} + \frac{\Delta V_{c,hydr}}{V_{c0}}\right)^3 \\ &= \kappa_0 \left(1 + \frac{p_c(t)}{K_{c,p}} + \frac{\sigma_0(t)}{K_{c,\sigma}} + J_{\delta_c}(t) \otimes c_{edge}(t)\right)^3 \end{aligned} \quad (23)$$

where $c_{edge}(t) = c_{edge}(p_c(t))$, as given by Eq. (5). Note that, although the variations of volume ΔV_c satisfy Boltzmann superposition principle when expressed versus the amount of adsorbed fluid on the edge of the cleat, the variations of permeability do not. Likewise, when expressed versus the pressure p_c of the fluid in the cleats, the variations of volume ΔV_c do not satisfy the Boltzmann superposition principle.

Note that the amount $m_m(t)$ of fluid in the coal matrix (per unit volume V_0 of fractured coal in the reference configuration), as well as the flux $\dot{m}_m(t)$ of fluid from the cleats to the coal matrix (still per unit volume V_0 of fractured coal in the reference configuration), also satisfy the Boltzmann superposition principle, so that one can write:

$$m_m(t) = J_{m_m}(t) \otimes c_{edge}(t) = \int_{\tau=-\infty}^{t} J_{m_m}(t-\tau) \frac{\partial c_{edge}}{\partial \tau}(\tau) d\tau \quad (24)$$

and:

$$\dot{m}_m(t) = J_{\dot{m}_m}(t) \otimes c_{edge}(t) = \int_{\tau=-\infty}^{t} J_{\dot{m}_m}(t-\tau) \frac{\partial c_{edge}}{\partial \tau}(\tau) d\tau \quad (25)$$

where $J_{m_m}(t)$ and $J_{\dot{m}_m}(t)$ are two kernels which verify:

$$J_{\dot{m}_m}(t) = dJ_{m_m}/dt \quad (26)$$

The three kernels $J_{\delta_c}(t)$, $J_{m_m}(t)$, and $J_{\dot{m}_m}(t)$ are displayed in Figure 9 for the various geometries of cleats. For what concerns the variation of aperture $\Delta V_{c,mech}(t)/V_{c,0}$ due to the

mechanical pressure of the fluid in the cleat (see Eq. (16)), the stiffness $K_{c,p}$ can be directly calculated from the numerical simulations of individual cleats performed in section 2.2. This stiffness characterizes how much the cleat's volume increases instantaneously when the fluid pressure in the cleat increases. From those simulations, we find that the stiffness $K_{c,p}$ is equal to 104.2 MPa, 381.1 MPa, 1.121 GPa, 2.558 GPa, for the cleats with an elliptical cross-section with aspect ratio $a/A = 0.03, 0.1, 0.3, 1$, respectively, and to 161.3 MPa for the cleat with rectangular cross-section. We observe that the shape of the cleat seems to have little effect on the time at which the aperture of the cleat is minimal, but has a significant effect on the magnitude of the transient variation of this aperture: the smaller the aspect ratio a/A, the more pronounced those variations are.

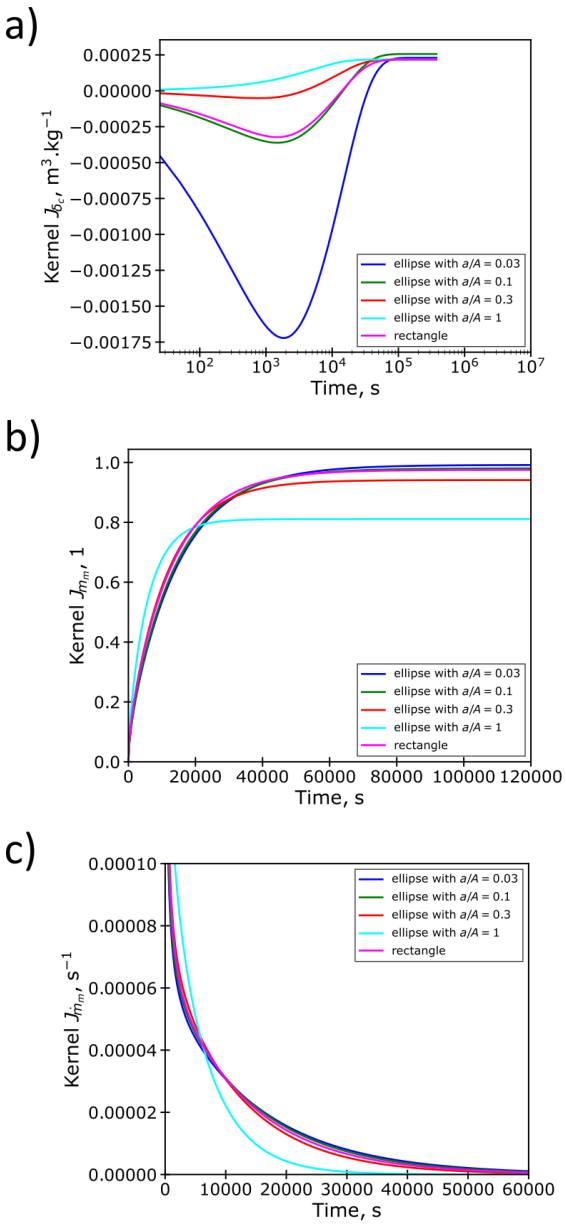

Figure 9: Kernels (a) $J_{\delta_c}(t)$, (b) $J_{m_m}(t)$, and (c) $J_{\dot{m}_m}(t)$ for all geometries of cleats, which define the response of the cleat in terms of relative volume variation $\Delta V_c(t)/V_0$, average amount $m_m(t)$ of fluid in the coal matrix per unit volume of fractured coal, and rate $\dot{m}_m(t)$

of variation of this same amount, respectively. The characteristic time τ used to make the time dimensionless is $\tau = 25{,}000\ s$.

2.4 A numerical verification of response of individual cleat to a generic loading

This section is dedicated to validating the approach proposed in section 2.3, based on the Boltzmann superposition principle, to calculate the response of an individual cleat to a generic history $p_c(t)$ of the pressure of fluid in the cleat. We perform the validation on the elliptical cleat with an aspect ratio $a/A = 0.03$ submitted to no confining stress (i.e., $\sigma_0 = 0$). The cleat is submitted to various histories $p_c(t)$ of the pressure of fluid. We calculate the cleat's response in two manners: 1) plane-strain finite-element calculations identical to the ones performed in section 2.2 but for the history $p_c(t)$ of the pressure of fluid in the cleat, and 2) calculations based on the method proposed in section 2.3 that uses the Boltzmann superposition principle. From both approaches, we obtain: the relative volume variation $\Delta V_c(t)/V_0$ of the cleat, the permeability $\kappa(t)$ over time (calculated from the relative volume variation $\Delta V_c(t)/V_0$ with Kozeny-Carman equation (3)), and the average amount $< c_m(t) >$ of fluid in the coal matrix per unit volume of coal matrix (with $< c_m(t) > = m_m(t)/(1 - \phi_{c,0})$, where $m_m(t)$ is the average amount of fluid in the coal matrix per unit volume of fractured coal). When aiming at using the Boltzmann superposition principle (section 2.3), the relative volume variation $\Delta V_c(t)/V_0$ and the average amount $m_m(t)$ of fluid in the coal matrix (per unit volume of fractured coal) are calculated with Eq. (15) (which uses Eqs. (16) and (21)) and Eq. (24), respectively, by using the kernels displayed in Figure 9.

We display the results of the comparison in Figure 10, Figure 11, and Figure 12, for what concerns the relative volume variation $\Delta V_c(t)/V_{c,0}$ of the cleat, the permeability $\kappa(t)$, and the average amount $< c_m(t) >$ of fluid in the coal matrix per unit volume of coal matrix, respectively. All calculations performed with Boltzmann superposition principle are in perfect agreement with the finite-element calculations, which validates the applicability of this former method introduced in section 2.3.

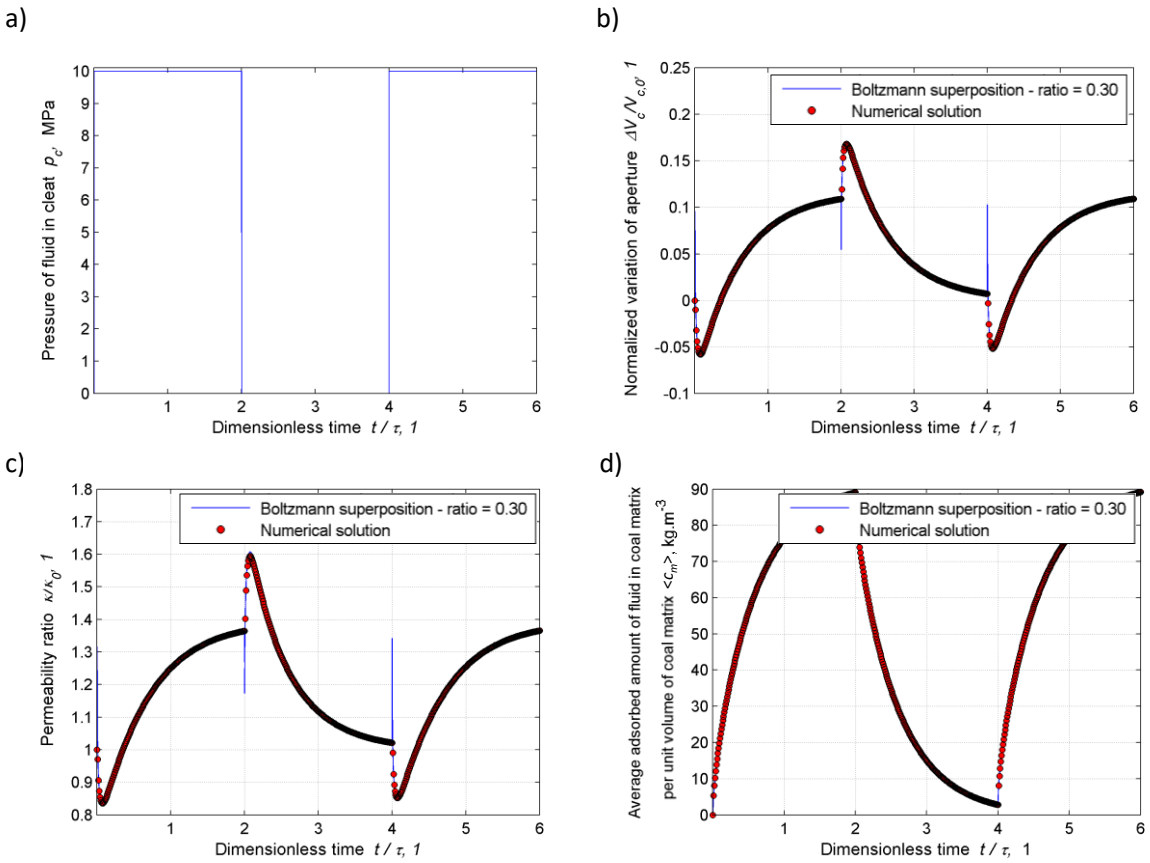

419

420 *Figure 10: Response of an individual elliptical cleat with an aspect ratio $a/A = 0.03$ to a*
421 *periodic rectangular loading: (a) history $p_c(t)$ of pressure of fluid considered, (b) variation*
422 *$\Delta V_c(t)/V_0$ of the relative volume of the cleat, (c) permeability $\kappa(t)$, and (d) average amount*
423 *$< c_m(t) >$ of fluid in the coal matrix per unit volume of coal matrix. The characteristic time τ*
424 *used to make the time dimensionless is $\tau = 25{,}000$ s.*

425

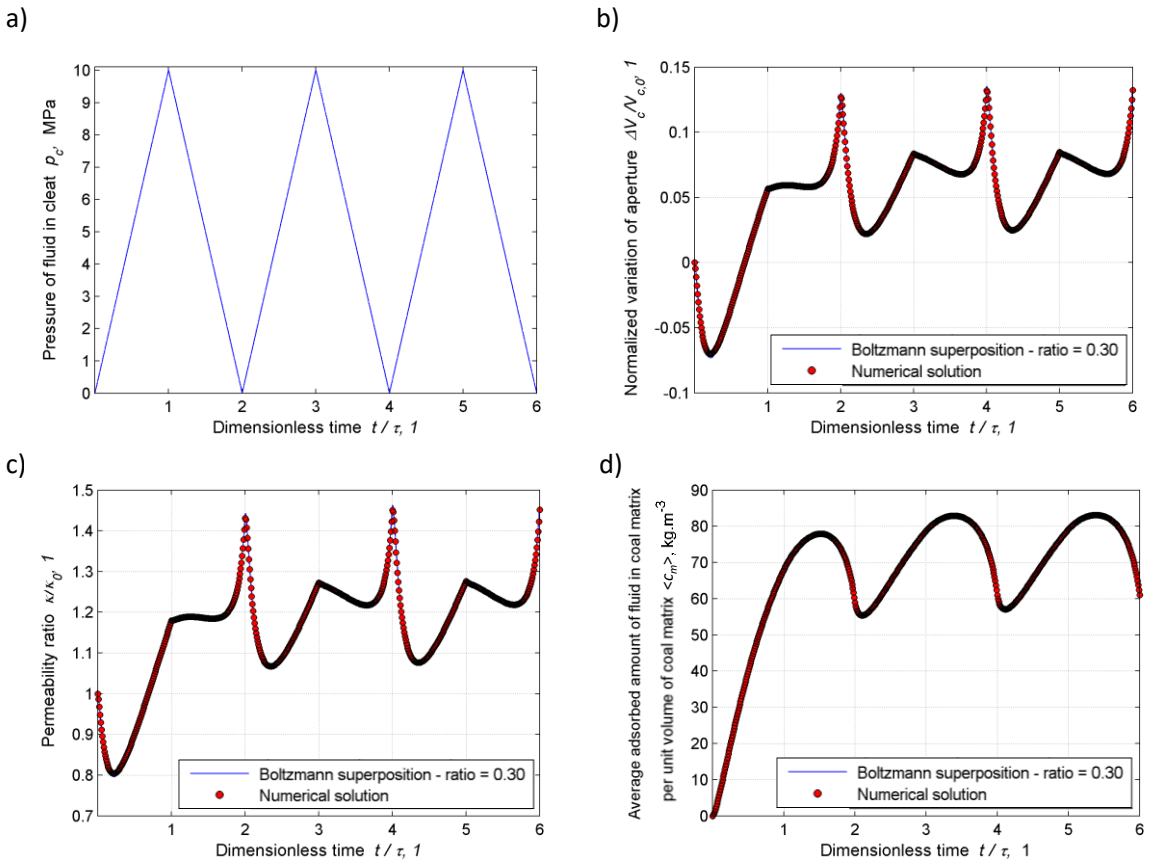

Figure 11: Response of an individual elliptical cleat with an aspect ratio $a/A = 0.03$ to a triangular loading: (a) history $p_c(t)$ of pressure of fluid considered, (b) variation $\Delta V_c(t)/V_0$ of the relative volume of the cleat, (c) permeability $\kappa(t)$, and (d) average amount $< c_m(t) >$ of fluid in the coal matrix per unit volume of coal matrix. The characteristic time τ used to make the time dimensionless is $\tau = 25{,}000$ s.

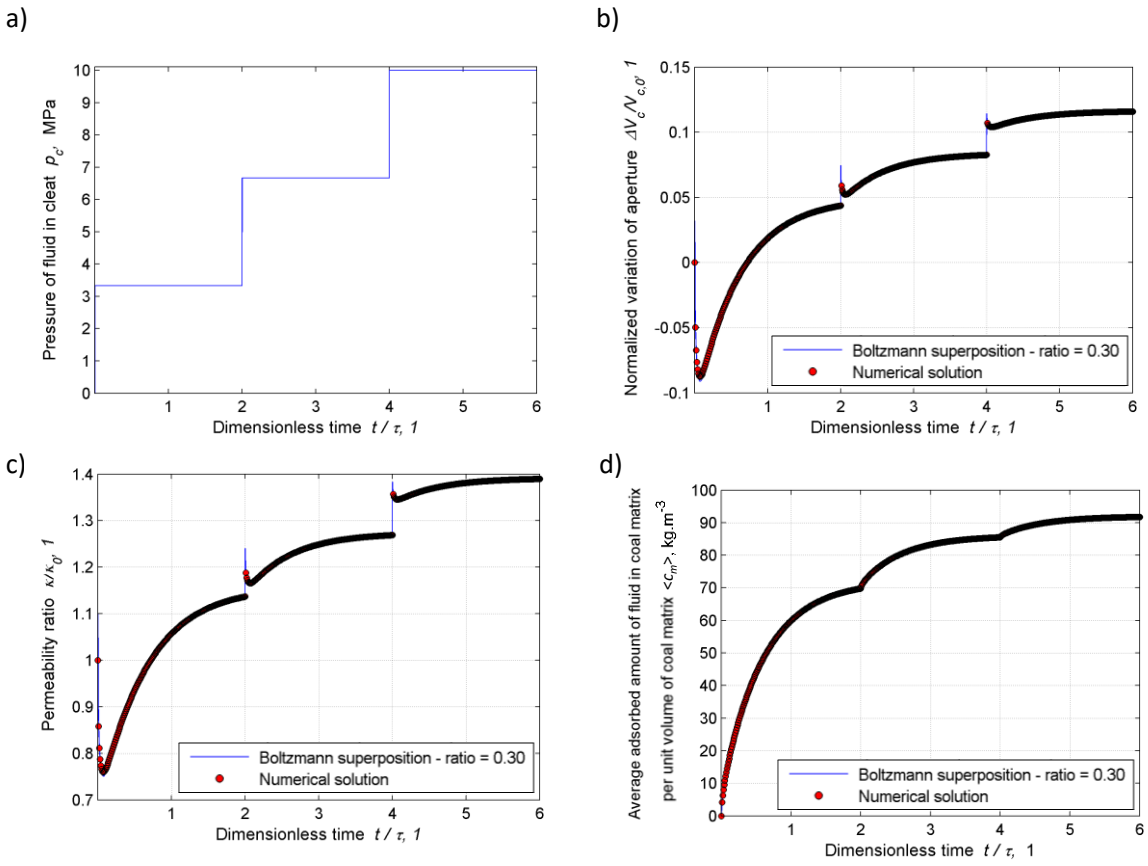

Figure 12: Response of an individual elliptical cleat with an aspect ratio $a/A = 0.03$ to a staircase loading: (a) history $p_c(t)$ of pressure of fluid considered, (b) variation $\Delta V_c(t)/V_0$ of the relative volume of the cleat, (c) permeability $\kappa(t)$, and (d) average amount $< c_m(t) >$ of fluid in the coal matrix per unit volume of coal matrix. The characteristic time τ used to make the time dimensionless is $\tau = 25{,}000$ s.

3 Modeling at the scale of the coal seam integrating transient variations of permeability obtained by FEM calculations at the scale of an individual cleat

We now consider the problem of an injection into a cylindrical coal structure of direction $\underline{e_x}$, of length $L = 200$ m, with an arbitrary cross-section whose characteristic dimension is much larger than the centimeter, so that there are many cleats over the cross-section (see Figure 13). The cleat with an elliptic cross-section of aspect ratio $a/A = 0.03$ considered in section 2 is assumed to be representative of the cleats in the sample. The sample initially contains CO_2 at $p_{init} = 1$ MPa. At time $t = 0$ s, CO_2 is injected at one end of the cylinder at a pressure $p_{inj}(t) = 10$ MPa while the other end and the lateral surface remain sealed. The process is assumed isothermal, remaining at 40°C. At this temperature, we consider an equation of state for CO_2 of the form:

$$\rho(p) = M_{CO_2}\left(\frac{p}{RT} + \frac{c_1}{1+\exp\left(-\left(\frac{p-c_2}{c_3}\right)\right)}\right) \quad (27)$$

where p is the pressure of the fluid, ρ is its mass density, $R = 8.314$ J.mol^{-1}.K^{-1} is the ideal gas constant, and c_1, c_2, c_3 are parameters. A fit of this equation to the actual equation of state of CO_2 at 40°C (Lemmon et al., 2020) yields $c_1 = 2.19 \cdot 10^4$ mol.m^{-3}, $c_2 = 9.92 \cdot 10^6$ Pa, and $c_3 = 1.21 \cdot 10^6$ Pa, with an error smaller than 12% over the whole range of pressures considered, even in supercritical conditions (i.e., above approximately 7.5 MPa). We consider that the properties of the material are those given in Table 1. We aim at solving the evolutions of the system over time.

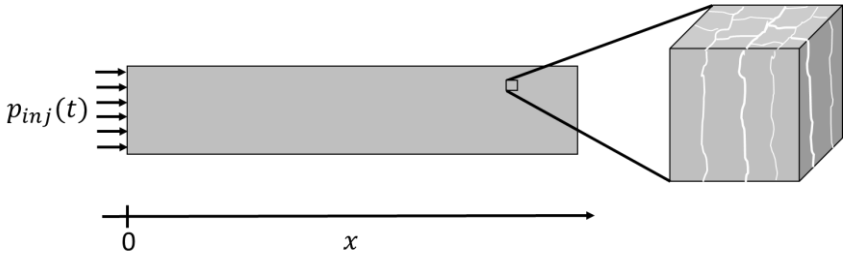

Figure 13: 1-dimensional problem solved at the scale of a structure. The inset is a zoom on a representative elementary volume. In the cleats, the fluid pressure is $p(x,t)$.

The initial hydraulic conditions read:

$$p_c(x,0) = p_{init}, \quad (28)$$

and the hydraulic boundary conditions read:

$$\begin{cases} p_c(x=0,t) = p_{inj}(t) = 10 \text{ MPa} \\ \left.\frac{\partial p_c}{\partial x}\right|_{x=L} = 0 \end{cases}. \quad (29)$$

We assume that the hydro-mechanical response of any representative elementary volume of material to a history of pressure $p_c(x,t)$ of fluid in the cleats is the same as the one identified with the Abaqus calculations performed in section 2 for a system containing an individual cleat. We will study the hydro-mechanical response of a representative elementary volume subjected to generic mechanical boundary conditions in section 4.

The problem considered is one-dimensional: at any time, all variables depend on the coordinate x only. Consequently, solving the problem means, in particular, finding out the evolutions in time of the pressure $p_c(x,t)$ of fluid in the cleat, of the average amount $m_m(x,t)$ of fluid in the coal matrix (per unit volume of fractured coal), and the permeability $\kappa(x,t)$. Since the fluid is injected from one end of the sample, in the generic case, the pressure $p_c(x,t)$ is expected to be heterogeneous, and hence the parameters $m_m(x,t)$ or $\kappa(x,t)$ as well. We expect the degree of heterogeneity and how heterogeneity remains to depend on the permeability κ_0 of the fractured coal: we will vary this parameter from $\kappa_0 = 10^{-13}$ m^2 to $\kappa_0 = 10^{-11}$ m^2 (which corresponds to the low permeability domain of Moore (2012)), while keeping other properties (see Table 1) constant.

Solving the problem requires first formulating the fractured coal's constitutive equations, the next section's focus.

3.1 Governing equations at the scale of the coal seam

We can write the mass balance equation for a representative elementary volume of fractured coal as:

$$\frac{\partial m}{\partial t} = -\frac{\partial w}{\partial x}, \tag{30}$$

where w is the macroscopic fluid mass flow through the cleat and m is the total fluid mass content (per unit volume V_0 of fractured coal in the reference configuration) which is composed of the fluid mass content m_c in the cleat and the fluid mass content m_m in the coal matrix (still per unit volume V_0 of fractured coal in the reference configuration), i.e., $m = m_c + m_m$.

The macroscopic flow (i.e., transfer of mass) of fluid through the cleats (also called seepage) is a viscous flow generally considered (Harpalani and Chen, 1997) to obey Darcy's law (Darcy, 1856):

$$w(x,t) = -\frac{\rho_F \kappa}{\eta_F}\frac{\partial p_c}{\partial x} = -k\frac{\partial p_c}{\partial x} \tag{31}$$

where $k = \rho_F\kappa/\eta_F$, $p_c = p_c(x,t)$, $\kappa = \kappa(x,t)$, and where ρ_F and η_F are the bulk mass density and the viscosity of the fluid (here CO_2), respectively. Under isothermal conditions, $\rho_F = \rho_F(p_c)$. For CO_2, we consider the equation of state given in Eq. (*27*). We assume that the viscosity $\eta_F = 47.83 \cdot 10^{-3}$ Pa.s (which corresponds to the viscosity of CO_2 at 313.15K and 10 MPa (Lemmon et al., 2020)) does not depend on the pressure of the fluid.

The mass m_c of fluid in the cleat is related to the cleat porosity ϕ_c through $m_c = \rho_F\phi_c$. Assuming that the variations of the mass of fluid in the cleat due to the deformation of the cleat are negligible when compared to variations of mass due to variations of density, the mass m_c of fluid in the cleats can be written as follows:

$$m_c = \rho_F\phi_{c,0} \tag{32}$$

We neglect microscopic flow through the coal matrix in the direction (Ox) (i.e., $\underline{w}_m.\underline{e}_x = 0$). Therefore, one can adapt Eq. (24) as follows:

$$m_m(x,t) = J_{m_m}(t) \otimes c_{edge}(x,t) \tag{33}$$

Likewise, for what concerns the evolutions of permeability, by taking into account that $\sigma_0 = 0$, we can adapt Eq. (23) as:

$$\kappa(x,t) = \kappa_0\left(1 + \frac{p_c(x,t)}{K_c} + J_{\delta_c}(t) \otimes c_{edge}(x,t)\right)^3 \tag{34}$$

where $c_{edge}(x,t) = c_{edge}(p_c(x,t))$, as given by Eq. (5).

The kernels $J_{\delta_c}(t)$ and $J_{\dot{m}_m}(t)$ required for the computation are those displayed in Figure 9 for the elliptical cleat with an aspect ratio $a/A = 0.03$.

3.2 Resolution of the problem with finite volume method

We divide space into $N_{nodes}+1$ equispaced nodes, with node 0 located in $x_0 = 0$ and node N_{nodes} located in $x_{N_{nodes}} = L$. We note $d_{ij} = L/N_{nodes}$ the distance between neighboring nodes i and j. We note all variables at node i with a subscript i. We note the time step Δt.

We obtain the finite volume scheme by a discrete balance in the elements of the mesh. Integrating Eq. (30) over any element i of length V_i and discretizing it in time with a backward Euler scheme yields, for all elements i:

$$V_i\big(m_i(t+\Delta t) - m_i(t)\big) + \Delta t \sum_j w_{ij}(t+\Delta t) = 0 \tag{35}$$

where w_{ij} expresses an approximation of the outflow from element i to element j for any i and any neighbor j of i:

$$w_{ij}(t+\Delta t) = -\,k_{ij}(t)\frac{p_j(t+\Delta t) \;-\; p_i(t+\Delta t)}{d_{ij}} \tag{36}$$

where d_{ij} is the distance between the center of element i and element j. In this equation k_{ij} is an explicit evaluation of the permeability coefficient $k \;= \rho_F \kappa/\eta_F$ at the interface between element i and element j, here $k_{ij} = (k_i + k_j)/2$.

At node 0, the pressure is imposed:

$$p_0(t+\Delta t) - p_{inj} = 0 \tag{37}$$

Equation (35) is solved through an iterative process. Since m_m is a functional of $c(t)$, we have to evaluate the change δm_m for any change δc between t and $t+\Delta t$:

$$\delta m_m = \int_t^{t+\Delta t} J_{m_m}(t+\Delta t-u)\frac{\partial}{\partial u}(\delta c)\,du \tag{38}$$

Approximating δc by $\delta[c(t+\Delta t)]\;(u-t)/\Delta t$ between t and $t+\Delta t$, we finally get:

$$\delta m_m = \left(\frac{1}{\Delta t}\int_0^{\Delta t} J_{m_m}(\Delta t-u)\,du\right)\delta c(t+\Delta t) \approx J_{m_m}(\,\Delta t)\,\delta c(t+\Delta t)/2 \tag{39}$$

So, the set of equations (35), formally $E_i = 0$ for all $i \geq 1$, can be solved iteratively through a Newton method, $A_{ij}\delta p_j = -\,E_i$, and using the jacobian matrix:

$$\begin{aligned} A_{ij} = V_i\left(\phi_{c,0}\frac{d\rho_F}{dp_i} + \frac{J_{m_m}(\Delta t)}{2}\,\frac{dc_{edge}}{dp_i}\right)\delta_{ij} \\ + \Delta t\left(\left(\sum_{r\in\text{neighbors}}\frac{k_{ir}(t)}{d_{ir}}\right)\delta_{ij} - \frac{k_{ij}(t)}{d_{ij}}\right) \end{aligned} \tag{40}$$

The Python code to solve this problem is available on the GitHub repository of the corresponding author[2].

[2] If you base future research on this code, please acknowledge it appropriately in your publications and cite the present article.

3.3 Results and discussion of the various kinetics involved

We display the results in Figure 14, Figure 15, and Figure 16 for the samples with a reference permeability κ_0 equal to 10^{-11} m^2, 10^{-12} m^2 and 10^{-13} m^2, respectively. Note that the times at which we display the results vary from figure to figure since the pressure in the cleats needs more time to reach its asymptotic value when the permeability κ_0 is lower.

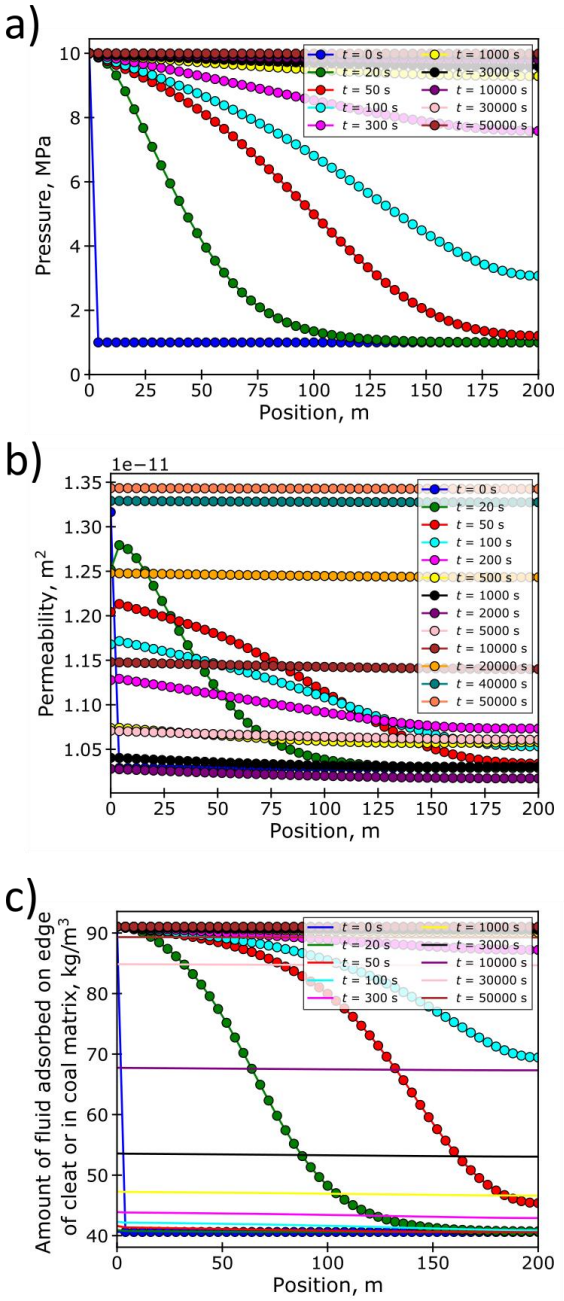

Figure 14: Distribution of (a) pressure p_c in cleats, (b) permeability κ, and (c) concentrations of adsorbed fluid during injection into a coal sample with a reference permeability $\kappa_0 = 10^{-11}$ m². In sub-figure c are displayed the concentration c_{edge} of fluid adsorbed on the edge of the cleat (with symbols) and the average concentration $< c_m >$ of fluid adsorbed in the coal matrix (with solid lines). Both concentrations are expressed per unit volume of the coal matrix.

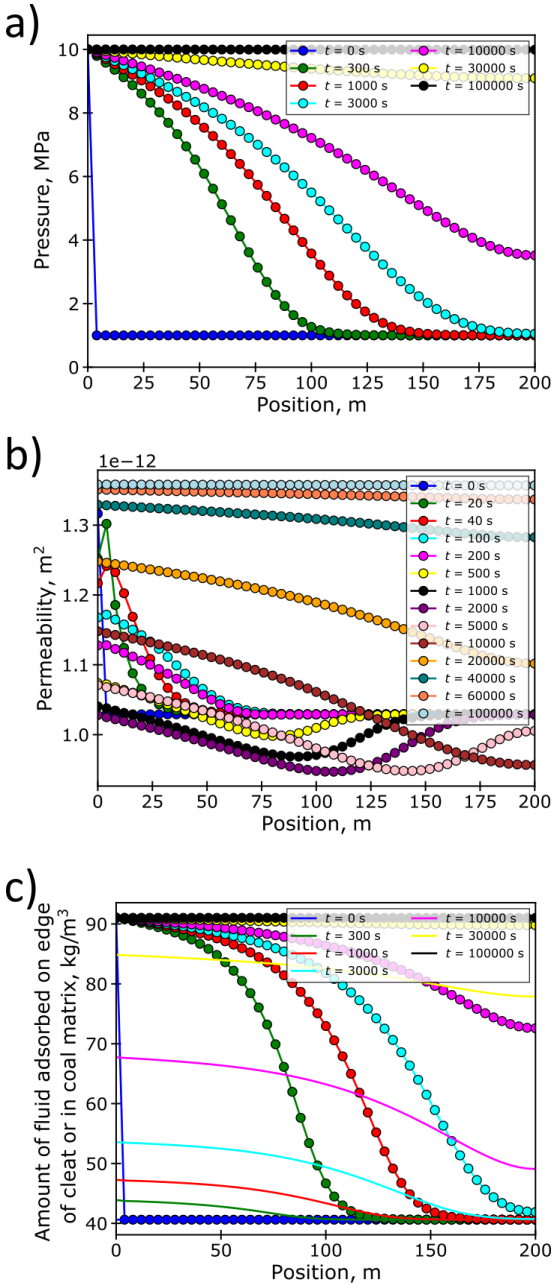

Figure 15: Distribution of (a) pressure p_c in cleats, (b) permeability κ, and (c) concentrations of adsorbed fluid during injection into a coal sample with a reference permeability $\kappa_0 = 10^{-12}$ m². In sub-figure c are displayed the concentration c_{edge} of fluid adsorbed on the edge of the cleat (with symbols) and the average concentration $< c_m >$ of fluid adsorbed in the coal matrix (with solid lines). Both concentrations are expressed per unit volume of the coal matrix.

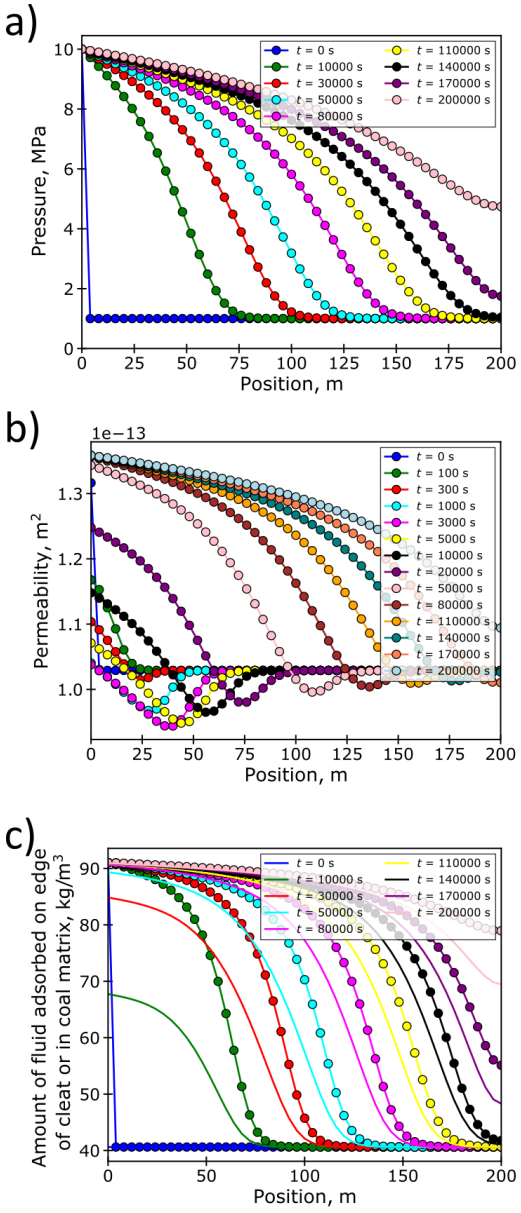

Figure 16: Distribution of (a) pressure p_c in cleats, (b) permeability κ, and (c) concentrations of adsorbed fluid during injection into a coal sample with a reference permeability $\kappa_0 = 10^{-13}$ m². In sub-figure c are displayed the concentration c_{edge} of fluid adsorbed on the edge of the cleat (with symbols) and the average concentration $< c_m >$ of fluid adsorbed in the coal matrix (with solid lines). Both concentrations are expressed per unit volume of the coal matrix.

One can observe different behaviors depending on the permeability κ_0. For the system with the highest permeability $\kappa_0 = 10^{-11}$ m² (see Figure 14), the pressure p_c in the cleats becomes homogeneous before a significant amount of fluid has diffused into the coal matrix (since at time $t = 1000$ s, the average concentration $< c_m >$ of fluid in the coal matrix is still low almost everywhere in the sample (see Figure 14-c)). Consequently, diffusion in the coal matrix mostly happens after the pressure in the cleats has become homogeneous. The average amounts of fluid adsorbed in the coal matrix and the transient adsorption-induced

variations of permeability are relatively homogeneous compared to the concentration on the edge of the cleats. Also, the evolution of the permeability over time is rather complex, as it is nonmonotonic and shaped like the letter N (i.e., it increases, decreases, and then increases back). In contrast, for the system with the lowest permeability $\kappa_0 = 10^{-13}$ m^2 (see Figure 16), transfer of fluid from/to the coal matrix happens faster than transport of fluid through the cleat system: when the pressure in the cleats becomes homogeneous, the system has reached equilibrium. One can check that, during the injection, at any position $x > 100$ m and at any time t, the average concentration of fluid in the coal matrix is relatively close to the one given by Eq. (5), i.e., relatively close to the concentration of fluid adsorbed on the cleat's edge. Locally, for all those positions, we always remain relatively close to local thermodynamic equilibrium. Far from the injection point, the permeability almost increases monotonically with time while displaying the same pattern of heterogeneity as the pressure. Finally, the system with the intermediate permeability $\kappa_0 = 10^{-12}$ m^2 (see Figure 15) manifests a behavior that is intermediate between the one observed for the system with permeability $\kappa_0 = 10^{-11}$ m^2 (see Figure 14) and $\kappa_0 = 10^{-13}$ m^2 (see Figure 16).

The results show a competition between two kinetics: 1) advective transfer through the cleat network and 2) diffusive exchange between cleats and coal matrix. A characteristic time τ_{diff} of diffusion of fluid from the cleats to the coal matrix is:

$$\tau_{diff} = (L_{diff})^2/D, \tag{41}$$

where L_{diff} is a characteristic drainage length around each cleat (and is therefore equal to half a characteristic distance between cleats). In the simulations at the scale of an individual cleat performed in section 2, for which $L_{diff} \sim 0.5 \times 10^{-2}$ m, we find $\tau_{diff} \sim 2.5 \times 10^4$ s.

We define a characteristic time τ_{advec} of the advective transfer through the cleats network as the characteristic time required for the pressure on the edge of the reservoir to be disturbed by the injection. We can obtain this characteristic time readily from an observation of Figure 14, Figure 15, and Figure 16: we find that $\tau_{advec} \sim 1 \cdot 10^2$ s, $\tau_{advec} \sim 1 \cdot 10^4$ s, and $\tau_{advec} \sim 1 \cdot 10^5$ s, for the systems with $\kappa_0 = 1 \cdot 10^{-11}$ m^2, $\kappa_0 = 1 \cdot 10^{-12}$ m^2, and $\kappa_0 = 1 \cdot 10^{-13}$ m^2, respectively.

From the orders of magnitude just calculated, we infer that the assumption of local thermodynamic equilibrium is reasonably valid if:

$$\tau_{advec} \gg \tau_{diff}. \tag{42}$$

In such a case, transient variations of permeability occur on the time scale τ_{diff}, which is too short to impact the transfer process at the structural scale (which occurs on the time scale τ_{advec}) significantly. At all positions that verify this criterion, at any time t, the average concentration $< c_m >$ of fluid in the coal matrix is relatively close to the one given by Eq. (5). In contrast, if τ_{advec} is not much larger than τ_{diff}, the assumption of local thermodynamic equilibrium is not valid anymore, and transient variations of permeability can impact the dynamics of transfer at the structural scale (if the magnitude of those variations is significant). The results displayed in Figure 14 to Figure 16 support this discussion regarding the various kinetics involved in the process: only in the system with reference permeability $\kappa_0 = 1 \cdot 10^{-13}$ m^2 and further from about 100 m from the point of injection is the condition (42) respected and the assumption of local thermodynamic equilibrium appears to be reasonably valid.

In contrast, in the case where $\tau_{advec} \ll \tau_{diff}$, the fluid has time to flow through the cleats before diffusing significantly through the coal matrix. The transient variations of permeability occur once the pressure of fluid in the cleats has become homogeneous. Consequently, the transient variations of permeability occur homogeneously as well.

4 Modeling at the scale of the coal seam integrating transient variations of permeability: an engineering approach

In section 3, we showed that one could perform calculations at the structural scale as soon as two kernels are known: the kernel $J_{\delta_c}(t)$ that governs how the volume or aperture of the cleats varies over time and the kernel $J_{\dot{m}_m}(t)$ that governs the rate at which fluid is being transferred from the cleats to the coal matrix. We obtained those kernels through finite-elements simulations in section 2.3. However, the need to resort to finite-element simulations of a representative cleat is impractical for the engineer, who first of all does not know the cleats' geometry. To respond to this issue, in this section, we propose a generic form for those kernels.

In section 2, also, we performed all calculations in plane-strain. In this section, we derive constitutive equations of a representative elementary volume of fractured coal submitted to a generic state of strains and stresses to give more flexibility to use the proposed model.

Finally, up to now, we considered exclusively that variations of permeability are due to variations of aperture or volume of the cleat through the Kozeny-Carman relationship (3). However, instead of using Kozeny-Carman-type laws to model permeability in coal, many use stress-based permeability laws. This section also explains how to model transient variations of permeability when using those latter permeability laws.

4.1 Constitutive equations of a representative elementary volume of fractured coal including transient variations of permeability under a generic state of strains or stresses

We consider a representative elementary volume of isotropic fractured coal under a generic state of strains or stresses. Suppose the coal matrix fluid is homogeneously distributed (without needing necessarily to be in equilibrium with the fluid in the cleats). Under the assumption that deformations have a negligible impact on the amounts of fluid in the cleats and the coal matrix, the poromechanical behavior of this representative elementary volume is given by (Espinoza et al., 2016):

$$\begin{cases} \sigma = K\varepsilon - bp_c - (1-b)\sigma^a(c_m) \\ s_{ij} = 2Ge_{ij} \\ \phi_c - \phi_{c,0} = b\varepsilon + \frac{p_c}{N} - \frac{\sigma^a(c_m)}{N} \\ m_T = \phi_{c,0}\rho_F(p_c) + (1-\phi_{c,0})c_m \end{cases}, \tag{43}$$

where c_m is the mass of fluid in the coal matrix per unit volume of coal matrix (such that $m_m = (1-\phi_{c,0})c_m$, since m_m is the mass of fluid in the coal matrix per unit volume of fractured coal); m_T is the total mass of fluid in the fractured coal per unit volume of fractured coal; σ, s_{ij}, ε, and e_{ij} are the volume stress, shear stresses, volume strain, and shear strains,

643 respectively; K, G, b, and N are the bulk modulus, shear modulus, Biot coefficient, and Biot
644 modulus, respectively; σ^a is the adsorption stress that intervened in Eq. (9).

645 As explained in section 2, transient variations of permeability are due to the fluid
646 distribution's heterogeneity in the coal matrix. To capture those transient effects, we,
647 therefore, propose to extend the set of Eqs. (43) into:

$$\begin{cases} \sigma = K\varepsilon - bp_c - (1-b)\sigma^a(< c_m >) \\ s_{ij} = 2Ge_{ij} \\ \phi_c - \phi_{c,0} = b\varepsilon + \dfrac{p_c}{N} - \dfrac{\sigma^a(< c_m >)}{N} + \Delta\phi_{c,t} \\ m_T = \phi_{c,0}\rho_F(p_c) + \left(1-\phi_{c,0}\right) < c_m > \end{cases} \quad (44)$$

648 where $< c_m >$ denotes the volume average of c_m over the coal matrix, and where the
649 function $\Delta\phi_{c,t}$ captures the transient variations of the porosity associated with the cleat
650 system. Note that, like in section 3.1, these functions neglect the impact of deformation on
651 the fluid amounts.

652 With the same reasoning as the one performed in section 2.3, we can obtain the average
653 amount $< c_m >$ of fluid in the coal matrix through convolution:

$$< c_m(t) >= J_{<c_m>}(t) \otimes c_{edge}(t) \quad (45)$$

654 where the function $J_{<c_m>}(t)$ is a kernel. Since $m_m(t) = (1-\phi_{c,0}) < c_m(t) >$, we have
655 $J_{<c_m>}(t) = J_{m_m}(t)/(1-\phi_{c,0})$. Given the shape of the kernel $J_{m_m}(t)$ (see Figure 9-b), for the
656 kernel $J_{<c_m>}(t)$ we propose the function:

$$J_{<c_m>}(t) = 1 - \exp(-t/\tau_{diff}), \quad (46)$$

657 where τ_{diff} is the characteristic time for the fluid in the representative elementary volume to
658 diffuse through the coal matrix. This kernel tends toward one at large times and thus verifies
659 that when a step of concentration $c_{edge,0}$ is applied on the edge of the cleat, at large times,
660 the average concentration of fluid in the coal matrix tends toward $c_{edge,0}$.

661 Because of the presence of the term $< c_m(t) >$, the set of equations (44) includes some
662 dependency versus time, such that the porous solid behaves apparently like a poroviscoelastic
663 solid. Consequently, we could rewrite this set of equations in the framework of a functional
664 approach to poroviscoelasticity (Coussy, 2004) by introducing an apparent relaxation bulk
665 modulus $K(t)$, a shear modulus $G(t)$, and a Biot coefficient $b(t)$, but such rewriting is out of
666 the scope of this study, which is focused on the modeling of transient evolutions of
667 permeability mostly.

668 In Eq. (44), variations $\phi_c - \phi_{c,0}$ of cleat porosity are composed of various terms: 1)
669 terms that depend on time-independent variables, 2) a term that takes into account the
670 average swelling of the coal matrix and takes into account the history of concentration, 3) a
671 transient term $\Delta\phi_{c,t}$. Again, we can assert that this transient variation $\Delta\phi_{c,t}$ of the cleat pore
672 volume can be obtained through a convolution product:

$$\Delta\phi_{c,t} = J_{\phi_c}(t) \otimes c_{edge}(t) \quad (47)$$

where the function $J_{\phi_c}(t)$ is a kernel. For this kernel $J_{\phi_c}(t)$, we propose a function of the form:

$$J_{\phi_c}(t) = -\frac{\Delta\phi_{c,max}}{c_{m,max}} \exp(-t/\tau_{diff})(1 - \exp(-t/\tau_{closing}), \quad (48)$$

where it is reasonable to consider that the characteristic time τ_{diff} is the same as in the previous equation, where $\tau_{closing}$ is another characteristic time, related to the time for the cleat to reach its minimum aperture, and where the parameter $\Delta\phi_{c,max}$ controls the magnitude of the maximal reduction of the cleat's aperture.

When permeability is given by the Kozeny-Carman relationship (3), we have all equations needed to perform the calculations. In comparison with classical poromechanical formulations that disregard the transient phenomena here considered, to capture those transient phenomena, we need therefore to introduce two kernels, namely the function $J_{<c_m>}(t)$ that governs how the average concentration of fluid in the coal matrix varies and the function $J_{\phi_c}(t)$ that governs how the cleat porosity varies. To define those two kernels, we need only three parameters: the characteristic time τ_{diff} needed for the fluid to diffuse through the coal matrix (which is the only parameter required to define $J_{<c_m>}(t)$), a parameter $\Delta\phi_{c,max}$ that controls the magnitude of the maximal transient reduction of the cleat's aperture, and a characteristic time $\tau_{closing}$ for the cleat to reach its minimal aperture.

In contrast, when the permeability law is stress-based, we propose to adapt it into:

$$\kappa = \kappa_0 \exp(\sigma + p_c - \sigma_t) \quad (49)$$

where σ is the total volume stress and σ_t is a transient stress. We assume that we can obtain this transient stress through the following convolution product:

$$\sigma_t = J_\sigma(t) \otimes c_{edge}(t) \quad (50)$$

where, for the kernel $J_\sigma(t)$, we propose:

$$J_\sigma(t) = \frac{\sigma_{t,max}}{c_{m,max}} \exp\left(-t/\tau_{diff}\right)(1 - \exp(-t/\tau_{closing})) \quad (51)$$

where $\sigma_{t,max}$ is a parameter that controls the magnitude of the maximal transient stress. Note that, in the absence of sorption, Eq. (49) leads to a permeability of coal, which depends on the Terzaghi effective stress (as was considered analytically by Connell et al. (2010) or experimentally by Somerton et al. (1975), for instance). In contrast, by considering a Kozeny-Carman-type aperture-based permeability relationship (Eq. (1)), with the set of poroelastic equations (44), one instead finds that the permeability depends on the Biot effective stress.

Here again, in comparison with classical poromechanical formulations that disregard the transient phenomena here considered, to capture those transient phenomena, we need to use two kernels, namely the function $J_{<c_m>}(t)$ that governs how the average concentration of fluid in the coal matrix varies and the function $J_\sigma(t)$ that governs how the effective stress acting on the cleat porosity varies. To define those two functions, we need only three parameters: the characteristic time τ_{diff} for the fluid in the representative elementary volume to diffuse through the coal matrix, the characteristic time $\tau_{closing}$ for the cleat to reach

its minimum aperture and a characteristic maximal transient variation $\sigma_{t,max}$ of the effective stress acting on the cleat porosity.

4.2 Verification of the validity of the proposed kernels

As already explained in section 4.1, the kernel $J_{<c_m>}(t)$ that intervenes in Eq. (45) and was defined in Eq. (46) is related to the kernel $J_{m_m}(t)$ introduced in Eq. (24) through:

$$J_{m_m}(t) = (1 - \phi_{c,0}) J_{<c_m>}(t). \quad (52)$$

Consequently, given Eq. (26), we have:

$$J_{\dot{m}_m}(t) = \left(1 - \phi_{c,0}\right) dJ_{<c_m>}/dt. \quad (53)$$

The relation between the kernel $J_{\phi_c}(t)$ (that intervened in Eq. (47) and that we defined in Eq. (48)) and kernels introduced in section 2.3 is more complicated. An examination of the equation governing $\phi_c - \phi_{c,0}$ in the set of equations (44), together with the fact that the adsorption stress σ^a depends linearly on the average concentration $< c_m >$ in the coal matrix (see Eq. (9)), show that the kernel J_{ϕ_c} must depend linearly on the kernels J_{δ_c} and J_{m_m}. Given that the kernel J_{ϕ_c} captures variations of pore volume relative to the reference volume of porous solid (see Eq. (47)) while the kernel J_{δ_c} captures variations of pore volume relative to the reference pore volume (see Eq. (18)), we pose:

$$J_{\delta_c} = \frac{1}{\phi_{c,0}} J_{\phi_c} + \beta J_{m_m} \quad (54)$$

where β is a proportionality factor that we can calculate from the simulated kernels, as $\beta = \lim_{t \to +\infty} J_{\delta_c} / J_{m_m}$. Based on the simulations performed in section 2.2, for the elliptical cleat with aspect ratio $a/A = 0.03$, we find $\beta = 2.35 \cdot 10^{-4}$ m^3.kg^{-1}. Relation (54) explains that the kernel J_{ϕ_c} can converge toward 0 in the long term, while Figure 8-b displays a contribution $\Delta V_{c,hydr}$ to the variation of volume of the cleats that converges toward a strictly positive value: in Eq. (44), we capture this net increase of cleat volume due to hydric effects in the long term by terms other than $\Delta\phi_{c,t}$.

Based on these relations, we can assess the validity of the generic forms (46) and (48) proposed for the kernels $J_{<c_m>}(t)$ and $J_{\phi_c}(t)$. To do so, for each cleat geometry, we fit the parameters τ_{diff}, $\tau_{closing}$ and $\Delta\phi_{t,max}$ which define the kernels $J_{<c_m>}(t)$ and $J_{\phi_c}(t)$ so that the kernels $J_{m_m}(t)$ and $J_{\dot{m}_m}(t)$, $J_{\delta_c}(t)$, as calculated through relations (52), (53), and (54), respectively, are as close as possible from their numerical evaluation by finite-element calculations (see Figure 9). Note that, in this fit, all parameters other than τ_{diff}, $\tau_{closing}$ and $\Delta\phi_{t,max}$ that are required for the evaluation of the kernels (e.g., $c_{m,max}$ and $\phi_{c,0}$) are already known and can be found in Table 1.

We display the results of this fit for all cleat geometries in Figure 17 and give the fitted parameters in Table 2. The figure shows that the form chosen for the kernels $J_{<c_m>}(t)$ and $J_{\phi_c}(t)$ is appropriate, in the sense that those kernels can be successfully fitted to kernels obtained numerically with finite-element simulations of the explicit diffusion of the fluid through the coal matrix.

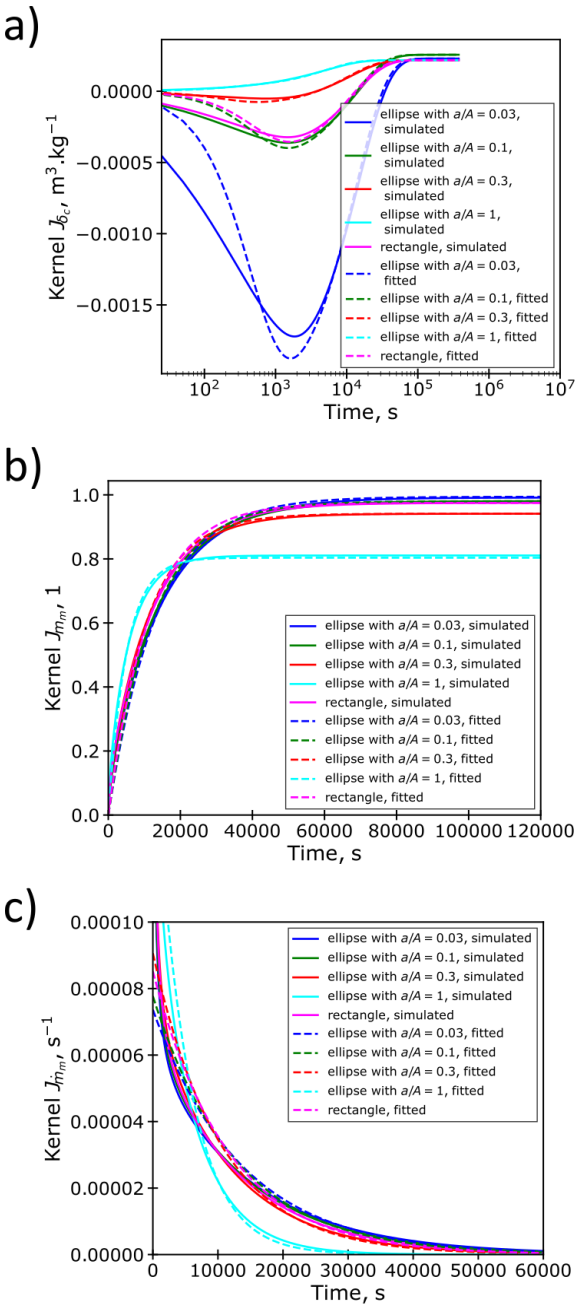

Figure 17: Kernels (a) $J_{\delta_c}(t)$, (b) $J_{m_m}(t)$, and (c) $J_{\dot{m}_m}(t)$ for all geometries of cleats considered in this study, as evaluated with finite-element simulations (solid lines) and as obtained by fitting the generic functions proposed for the kernels $J_{<c_m>}(t)$ and $J_{\phi_c}(t)$ (dashed lines).

Table 2: Results of fit of kernels $J_{<c_m>}(t)$ and $J_{\phi_c}(t)$

Geometry of cleat's cross-section	Characteristic time τ_{diff}, s	Characteristic time $\tau_{closing}$, s	Characteristic maximal reduction of cleat porosity $\Delta\phi_{c,max}$, 1
Elliptic with aspect ratio $a/A = 0.03$	13502.2	503.4	$1.390 \cdot 10^{-3}$
Elliptic with aspect ratio $a/A = 0.1$	12615.8	538.7	$1.064 \cdot 10^{-3}$
Elliptic with aspect ratio $a/A = 0.3$	10388.4	200.8	$6.085 \cdot 10^{-4}$
Elliptic with aspect ratio $a/A = 1$	5103.9	204.5	$-6.396 \cdot 10^{-4}$
Rectangular with aspect ratio $a/A = 0.1$	11447.5	600.1	$1.251 \cdot 10^{-3}$

The values provided in Table 2 make it possible to confirm an observation already given in section 2.2: the transient decrease of permeability (characterized by the parameter $\Delta\phi_{c,max}$) is all the more pronounced that the aspect ratio a/A of the cross section of the cleat differs from 1.0. The characteristic time τ_{diff} of the process of diffusion also decreases with an increasing aspect ratio a/A, but we believe that this effect is mostly due to the fact that, in our study, by construction, with an increasing aspect ratio a/A, the porosity of the cleats increases and hence the volume of coal matrix toward which fluid diffuses is lower. The magnitude of this characteristic time τ_{diff} is consistent with the value $L_{diff}^2/D = (0.5 \times 10^{-2}\ \mathrm{m}^2)^2/(10^{-9}\ \mathrm{m}^2.\mathrm{s}^{-1}) = 2.5 \cdot 10^4$ s expected from the inter-cleats spacing. Also, as already discussed in section 2.2, the characteristic time $\tau_{closing}$ is mostly independent of the aspect ratio when this aspect ratio differs sufficiently from 1 (i.e., when the cleat is flat enough). Figure 17 shows that this characteristic time $\tau_{closing}$ is about half-an-order-of-magnitude smaller than the actual time for the cleat to reach its minimal aperture (and hence for the permeability to be minimal). At a given aspect ratio, the three parameters are shown in Table 2, which define the various kernels, are roughly independent of the geometry of the cleat's cross-section, as can be inferred from an observation of the parameters for the elliptic and rectangular cleats with aspect ratio $a/A = 0.1$.

Parameters (e.g., permeability (Wold et al., 2008)) can vary significantly from the lab scale to the field scale. In the same spirit, the parameters proposed here in Table 2, obtained by calculations performed at the scale of an individual cleat, may differ from parameters relevant for calculations at the scale of the seam. However, Figure 17 shows that the kernels' form that we propose is valid for all geometries assumed for the cleat. Consequently, one could expect that this kernels' form should also be relevant for calculations performed at the seam scale, even though the three parameters that define the kernels quantitatively may differ from those given in Table 2. This difference must stem from the difference of scale and the fact that the actual cleats' geometry is not elliptical.

4.3 Example of calculation with the proposed kernels

In this section, we consider again the problem treated in section 3 of a one-dimensional injection into a cylindrical coal structure of length $L = 200$ m and of arbitrary cross section,

779 in which cleats with an elliptic cross-section of aspect ratio $a/A = 0.03$ is assumed to be
780 representative. We consider the same initial conditions (i.e., the sample contains CO_2 at 1
781 MPa) and hydraulic boundary conditions (i.e., CO_2 is injected at 10 MPa at one end of the
782 cylinder while the other surfaces remain sealed). However, in contrast to what we did in
783 section 3 in which we calculated the needed kernels with finite-element simulation, here we
784 use the kernels $J_{<c_m>}(t)$ and $J_{\phi_c}(t)$ given by Eqs. (46) and (48), respectively, together with
785 the fitted parameters given in Table 2 for the cleat of interest, i.e., $\tau_{diff} = 13502.2$ s,
786 $\tau_{closing} = 503.4$ s, and $\Delta\phi_{c,max} = 1.390 \cdot 10^{-3}$. The same code as in section 3.2 is used, but
787 now the kernels $J_{m_m}(t)$ and $J_{\dot{m}_m}(t)$, $J_{\delta_c}(t)$ are calculated from the kernels $J_{<c_m>}(t)$ and $J_{\phi_c}(t)$
788 through relations (52), (53), and (54). For such one-dimensional simulations, assuming like in
789 Section 3 that the hydro-mechanical couplings are all lumped in the proposed kernels, the
790 knowledge of Biot coefficient of Biot modulus is not needed. In contrast, generic 3-
791 dimensional simulations require those parameters.

792 The results of the simulation of the injection, displayed in Figure 18, compare well with
793 the results obtained with the kernels calculated with the finite-element simulations (see
794 Figure 15). Nevertheless, we observe some differences at the earliest times, when the
795 proposed kernels differ the most from the simulated ones (see Figure 17-a in particular).
796 However, the good agreement confirms that the generic form (46) and (48) of the kernels
797 $J_{<c_m>}(t)$ and $J_{\phi_c}(t)$ is appropriate to capture adsorption-induced transient variations of
798 permeability.

799

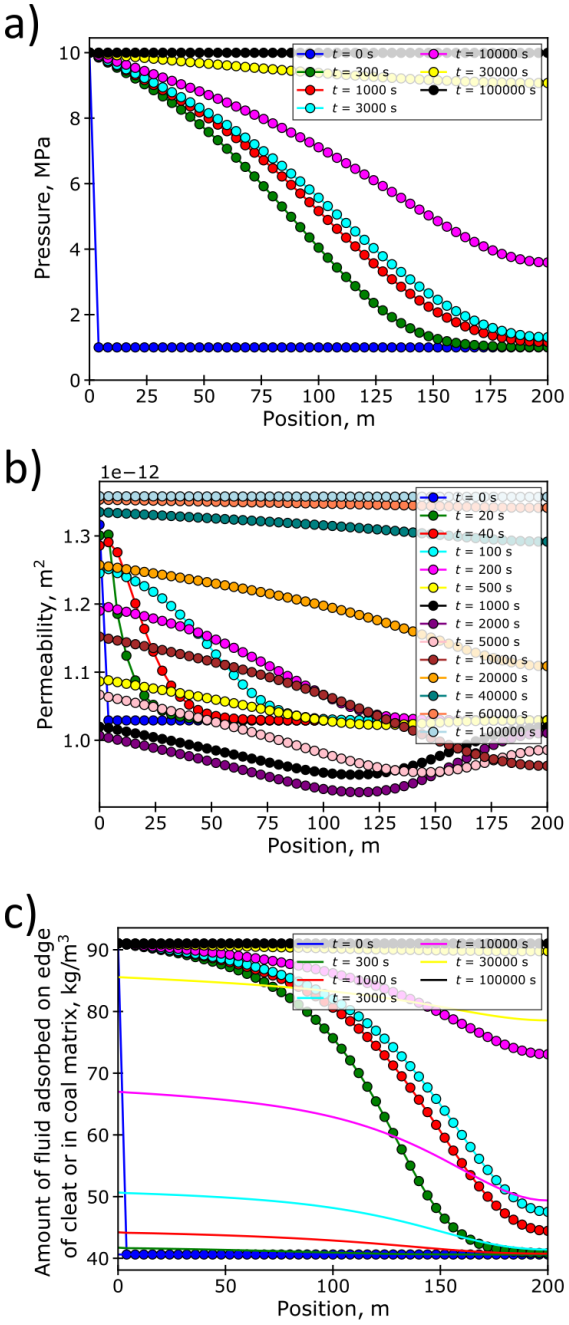

Figure 18: Distribution of (a) pressure p_c in cleats, (b) permeability κ, and (c) concentrations of adsorbed fluid during an injection in a coal sample with a reference permeability $\kappa_0 = 10^{-12}$ m^2, based on the generic kernels $J_{<c_m>}(t)$ and $J_{\phi_c}(t)$ given by Eqs. (46) and (48), respectively. For sub-figure c, the same comments apply as for Figure 15-c.

4.4 Limitations and perspectives

We identify the following limitations and perspectives:

- In the simulations of an injection of CO_2 into a coal sample or coal reservoir (see section 3), we made some assumptions to use the kernels calculated with finite-element simulations in section 2. Indeed, we assumed that fluid diffuses through the coal matrix only perpendicular to the cleats and neighboring slices do not restrain the swelling of a slice of coal perpendicular to the cleat. By relaxing those assumptions, the actual kernels to be used would differ from the ones calculated. But we do not expect the kernels' form to differ significantly from the generic forms proposed in section 4. Consequently, for the simulations performed in section 4.3, relaxing the assumptions above-mentioned would come back to use input parameters that would differ from the ones given in Table 2.
- The calculations that we performed in sections 3 and 4 at the scale of a coal sample or coal seam were based on the idea that some representative cleat exists. However, we know that the cleat system of coal seams is complex and somehow fractal, involving various geometries (i.e., shape, aperture, or aspect ratio) of the cleats and their spacing. Consequently, one should extend the approach presented in this work to such a case. We see no a priori impossibility in performing this extension. One could express the permeability of the representative elementary volume of fractured coal as a function of the aperture of the various families of cleats and could introduce kernels specific to each family of cleats.
- We discussed in section 3.3 the notion of local thermodynamic equilibrium. Depending on the coal's properties and the distance to the injection well, we found out that assuming local thermodynamic equilibrium could be reasonable or not. Even if, for a given coal seam, the assumption of local thermodynamic equilibrium is not valid at some locations in the seam or at some time during the injection process, assessing the quantitative impact of this assumption on the seam's response (in particular on the predicted flow rates) would be interesting.
- The proposed approach could be applied to other physical processes that induce heterogeneity inside the representative elementary volume of fractured coal. For instance, injection of a hot fluid would cause heterogeneity of temperature and thermal dilation inside the coal matrix and induce transient permeability variations. However, the approach here proposed, relying on the Boltzmann superposition principle, is limited to processes for which the time-dependent phenomena and their consequences can be expressed linearly. If nonlinearities enter the picture, then the method could be extended by introducing nonlinear convolutions in Volterra's formalism (Ogunfunmi, 2007). However, such formulation is significantly more complex than the one used in this study and requires a larger number of kernels, whose identification could prove difficult. As proposed in this study, as much as possible, aiming at formulating the governing equations linearly of the time-dependent physical process seems to be a reasonable approach to try before considering nonlinear developments.

5 Conclusions

In this work, we aimed at finding out how to model transient variations of permeability due to heterogeneous adsorption-induced swelling of the coal matrix by formulating constitutive equations at the scale of a representative elementary volume of fractured coal. The need to develop constitutive equations at this scale rather than at a lower scale stems from the will to perform simulations at the scale of a coal sample or a coal reservoir, without meshing explicitly coal matrix and cleat network and solving for the transport through the coal matrix. To better understand the physical processes involved, we first performed finite-element simulations of an individual cleat surrounded by a coal matrix, solving the transport of fluid through the coal matrix and the coal matrix's swelling. Then we derived the constitutive equations that we were seeking for, using the just mentioned finite-element calculations as inputs. Finally, we solved those constitutive equations with the finite-volume method to simulate CO_2 injection into a coal structure. The conclusions of this work are:

- We confirm that adsorption-induced transient variations of permeability can be due to the heterogeneity of the concentration of fluid in the coal matrix. The magnitude of those transient variations of permeability depends significantly on the aspect ratio of the cleat's cross-section (see Figure 5). In contrast, a characteristic duration τ_{diff} of those transient variations is relatively independent of the geometry of the cleat's cross-section (see Figure 5 again). This characteristic duration τ_{diff} should rather depend on the diffusivity D of the fluid through the coal matrix and on the characteristic distance L_{diff} between neighboring cleats (see Eq. (41)).
- Transient variations of permeability can be rigorously captured with constitutive equations formulated at the scale of a representative elementary volume of fractured coal. To do so, we relied on the Boltzmann superposition principle. The resulting constitutive equation (see Eq. (23)) involves a convolution product so that the permeability $\kappa(t)$ at a given time t depends on the full history of pressure $p_c(t')$ of fluid in the cleats until time t, i.e., at all times $t' < t$.
- Although transient adsorption-induced variations of permeability are involved, we could model them with a not-too-complex use of the Boltzmann superposition principle. The reason why we succeeded in doing so is the following: we can express the swelling as depending linearly on the concentration of fluid in the coal matrix (see Eq. (8)), and the transport of fluid through the coal matrix can be well modeled with a linear diffusion equation (see Eq. (7)) so that all-time dependent processes and their consequences depend linearly on the history $c_{edge}(t)$ of concentration of fluid in the coal matrix in the vicinity of the cleat. In this approach, all nonlinearity is concentrated into the instantaneous relation (5) between this concentration and the pressure $p_c(t)$ of the fluid in the cleats.
- At the scale of a representative elementary volume of fractured coal, to formulate a complete set of constitutive equations that can capture transient variations of permeability, we need to use convolutions productions that rely on

two kernels: one that governs the evolution of the aperture of the cleat (depending on how we write the equations, this kernel is $J_{\delta_c}(t)$ (see Eq. (34) in section 3.1) or $J_{\phi_c}(t)$ (see Eq. (47) in section 4.1) and one that governs the evolution of the amount of fluid in the coal matrix (depending on how we write the equations, this kernel is $J_{\dot{m}_m}(t) = dJ_{m_m}(t)/dt$ (see Eq. (33) in section 3.1) or $J_{<c_m>}(t)$ (see Eq. (45) in section 4.1)). Those two kernels can be identified with finite-element simulations of the transport of fluid through the coal matrix and the swelling it induces (see section 2.2 and Figure 9).

- At this same scale of a representative elementary volume of fractured coal, we proposed three-dimensional constitutive equations that can capture transient permeability variations in Eq. (44). Those constitutive equations require the knowledge of two kernels (i.e., $J_{\phi_c}(t)$ and $J_{<c_m>}(t)$), for which we propose generic forms (see Eqs. (46) and (48)) that can be used by the engineer. Altogether, those two kernels depend on only three parameters with an explicit physical meaning: a characteristic time τ_{diff} of diffusion of fluid through the coal matrix, a characteristic time $\tau_{closing}$ related to the closure of the cleats, and a parameter $\Delta\phi_{c,max}$ that controls the magnitude of the maximal transient variation of permeability. For those who prefer to model permeability as depending on stresses rather than on aperture of the cleat, we propose an appropriate adaptation of the permeability law (see Eq. (49)), which requires the knowledge of 1 kernel (see Eq. (50)) for which we also propose a generic form (see Eq. (51)) that also depends on three parameters with the same explicit physical meaning (i.e., the same two characteristic times and a parameter $\sigma_{t,max}$ that controls the magnitude of the maximal transient variations of effective stress).
- In the process of injection of fluid in a coal bed, two kinetics are at stake, namely the kinetics of advective transfer through the cleats (with a characteristic time τ_{advec}) and the kinetics of transfer from the cleats to the coal matrix (with a characteristic time τ_{diff}). If those characteristic times verify Eq. (42), i.e., $\tau_{advec} \gg \tau_{diff}$, local thermodynamic equilibrium is ensured: in a small representative elementary volume of fractured coal, one can consider that the chemical potential of the fluid is homogeneous (i.e., the same in the cleat as anywhere in the coal matrix). We provide an expression for the characteristic time τ_{diff} in Eq. (41). For a given system, it is possible that the assumption of local thermodynamic equilibrium could be valid far from the injection well but not reasonable in the vicinity of the injection well.

We discussed the limitations and perspectives in section 4.4.

Nomenclature

Symbol	Meaning	Unit
A_{ij}	Jacobian matrix	$kg.m^{-2}.Pa^{-1}$
a/A	Aspect ratio of elliptical cleat	1
α	Parameter governing magnitude of adsorption-induced swelling	$m^3.kg^{-1}$
b	Biot coefficient of fractured coal	1
β	Proportionality factor	$m^3.kg^{-1}$
c_{edge}	Amount of fluid adsorbed on edge of cleat	$kg.m^{-3}$
$\boldsymbol{C_m}$	Stiffness tensor of coal matrix	Pa
c_m	Mass concentration of fluid in coal matrix, per unit volume of coal matrix in reference configuration	$kg.m^{-3}$
$c_{m,max}$	Maximum adsorbed amount in Langmuir isotherm	$kg.m^{-3}$
D	Diffusivity of fluid in coal matrix	$m^2.s^{-1}$
$\partial\Omega_{in}$	Inner surface of system	N.A.
$\partial\Omega_{out}$	Outer surface of system	N.A.
$\Delta\phi_{c,t}$	Transient variations of porosity associated to cleat system	1
$\Delta\phi_{c,max}$	Maximal transient variation of porosity associated to cleat system	1
$\underline{\underline{e}}$	Shear strain tensor	1
$\underline{\underline{\varepsilon}}$	Strain tensor	1
ε	Volume strain	1
ε^a	Adsorption strain	1
ϕ_c	Porosity associated to cleats	1
η_F	Dynamic viscosity of fluid	Pa.s
$J_{<c_m>}$	Kernel associated to average mass concentration of fluid in coal matrix per unit volume of coal matrix	1
J_{δ_c}	Kernel associated to variation of aperture of cleats	$m^3.kg^{-1}$
J_{m_m}	Kernel associated to average mass concentration of fluid in coal matrix per unit volume of fractured coal	1
$J_{\dot{m}_m}$	Kernel associated to rate of variation of average mass concentration of fluid in coal matrix per unit volume of fractured coal	s^{-1}
J_{ϕ_c}	Kernel associated to variation of cleat porosity	$m^3.kg^{-1}$
J_σ	Kernel associated to transient stress	$Pa.m^3.kg^{-1}$
K	Bulk modulus of fractured coal	Pa
$K_{c,p}$	Parameter characterizing stiffness of cleat	Pa
$K_{c,\sigma}$	Parameter characterizing stiffness of cleat	Pa
K_m	Bulk modulus of coal matrix	Pa
k	Permeability coefficient	$kg.m^{-1}.Pa^{-1}.s^{-1}$
κ	Intrinsic permeability of fractured coal	m^2
κ_0	Intrinsic permeability of fractured coal in reference configuration	m^2
$\underline{\xi}$	Displacement	m
L	Length of system	m

M_F	Molar mass of fluid	kg.m^{-3}
M_{CO_2}	Molar mass of CO_2	kg.m^{-3}
m	Mass of fluid in fractured coal per unit volume of fractured coal	kg.m^{-3}
m_c	Mass of fluid in cleat per unit volume of fractured coal	kg.m^{-3}
m_m	Mass of fluid in coal matrix per unit volume of fractured coal	kg.m^{-3}
N	Biot modulus	Pa
$\underline{n}$	Outward normal vector	N.A.
ν_m	Poisson's ratio of coal matrix	1
p_c	Pressure of fluid in cleats	Pa
$p_{c,0}$	Step of pressure of fluid in cleats	Pa
p_{init}	Initial pressure of fluid in coal seam	Pa
p_{inj}	Pressure of injection in coal seam	Pa
p_{L0}	Characteristic pressure in Langmuir isotherm	Pa
p_m	Thermodynamic pressure of fluid in coal matrix	Pa
ρ_F	Mass density of fluid	kg.m^{-3}
R	Ideal gas constant	J.mol^{-1}.K^{-1}
$\underline{\underline{s}}$	Shear stress tensor	Pa
$\underline{\underline{\sigma}}$	Stress tensor	Pa
σ	Volume stress	Pa
σ^a	Adsorption stress	Pa
σ_0	Imposed confining stress	Pa
σ_t	Transient stress	Pa
$\sigma_{t,max}$	Characteristic maximal transient stress	Pa
t	Time	s
Δt	Time step	s
T	Temperature	K
τ	Characteristic time	s
τ_{advec}	Characteristic time of transfer through cleats network	s
$\tau_{closing}$	Characteristic time for cleats to reach their minimal aperture	s
τ_{diff}	Characteristic time of diffusion of fluid from cleats to coal matrix	s
V_c	Volume of cleats	m^3
$V_{c,0}$	Volume of cleats in reference configuration	m^3
V_0	Volume of fractured coal in reference configuration	m^3
V_i	Volume of element i	m
ΔV_c	Variation of volume of cleats	m^3
$\Delta V_{c,mech}$	Variation of volume of cleats due to mechanical effects	m^3
$\Delta V_{c,hydr}$	Variation of volume of cleats due to ingress of fluid in coal matrix	m^3
w	Mass flow rate of fluid through cleats	kg.m^{-2}.s^{-1}
w_m	Mass flow rate of fluid through coal matrix	kg.m^{-2}.s^{-1}
x	Position	m
Δx	Distance between nodes	m
Y	Heaviside function	1

933

References

Barenblatt, G.I., Zheltov, I.P., Kochina, I.N., 1960. Basic concepts in the theory of seepage of homogeneous liquids in fissured rocks [strata]. Journal of Applied Mathematics and Mechanics 24, 1286–1303.

Brochard, L., Vandamme, M., Pellenq, R.J.-M., 2012. Poromechanics of microporous media. Journal of the Mechanics and Physics of Solids 60, 606–622. https://doi.org/10.1016/j.jmps.2012.01.001

Chen, Z., Liu, J., Elsworth, D., Pan, Z., Wang, S., 2013. Roles of coal heterogeneity on evolution of coal permeability under unconstrained boundary conditions. Journal of Natural Gas Science and Engineering 15, 38–52. https://doi.org/10.1016/j.jngse.2013.09.002

Chen, Z., Liu, J., Pan, Z., Connell, L.D., Elsworth, D., 2012. Influence of the effective stress coefficient and sorption-induced strain on the evolution of coal permeability: Model development and analysis. International Journal of Greenhouse Gas Control 8, 101–110. https://doi.org/10.1016/j.ijggc.2012.01.015

Connell, L.D., Lu, M., Pan, Z., 2010. An analytical coal permeability model for tri-axial strain and stress conditions. International Journal of Coal Geology 84, 103–114. https://doi.org/10.1016/j.coal.2010.08.011

Coussy, O., 2010. Mechanics and Physics of Porous Solids. Wiley.

Coussy, O., 2004. Poromechanics. John Wiley & Sons. https://doi.org/10.1002/0470092718

Cui, X., Bustin, R.M., 2005. Volumetric strain associated with methane desorption and its impact on coalbed gas production from deep coal seams. AAPG Bulletin 89, 1181–1202. https://doi.org/10.1306/05110504114

Darcy, H., 1856. Les Fontaines Publiques de la Ville de Dijon. Victor Dalmont, Paris.

Espinoza, D.N., Vandamme, M., Dangla, P., Pereira, J.-M., Vidal-Gilbert, S., 2016. Adsorptive-mechanical properties of reconstituted granular coal: Experimental characterization and poromechanical modeling. International Journal of Coal Geology 162, 158–168. https://doi.org/10.1016/j.coal.2016.06.003

Espinoza, D.N., Vandamme, M., Pereira, J.-M., Dangla, P., Vidal-Gilbert, S., 2014. Measurement and modeling of adsorptive–poromechanical properties of bituminous coal cores exposed to CO2: Adsorption, swelling strains, swelling stresses and impact on fracture permeability. International Journal of Coal Geology 134–135, 80–95. https://doi.org/10.1016/j.coal.2014.09.010

Gale, J., 2004. Geological storage of CO2: What do we know, where are the gaps and what more needs to be done? Energy 29, 1329–1338. https://doi.org/10.1016/j.energy.2004.03.068

Gray, I., 1987. Reservoir Engineering in Coal Seams: Part 1-The Physical Process of Gas Storage and Movement in Coal Seams. SPE Reservoir Engineering 2, 28–34. https://doi.org/10.2118/12514-PA

Guo, P., Cheng, Y., Jin, K., Li, W., Tu, Q., Liu, H., 2014. Impact of effective stress and matrix deformation on the coal fracture permeability. Transport in Porous Media 103, 99–115. https://doi.org/10.1007/s11242-014-0289-4

Harpalani, S., Chen, G., 1997. Influence of gas production induced volumetric strain on permeability of coal. Geotech Geol Eng 15, 303–325. https://doi.org/10.1007/BF00880711

Harpalani, S., Schraufnagel, A., 1990. Measurement of parameters impacting methane recovery from coal seams. Geotechnical and Geological Engineering 8, 369–384. https://doi.org/10.1007/BF00920648

International Energy Agency, 2019. World energy balances: overview. International Energy Agency.
Izadi, G., Wang, S., Elsworth, D., Liu, J., Wu, Y., Pone, D., 2011. Permeability evolution of fluid-infiltrated coal containing discrete fractures. International Journal of Coal Geology 85, 202–211. https://doi.org/10.1016/j.coal.2010.10.006
Knorr, W., 2009. Is the airborne fraction of anthropogenic CO2 emissions increasing? Geophysical Research Letters 36. https://doi.org/10.1029/2009GL040613
Laubach, S.E., Marrett, R.A., Olson, J.E., Scott, A.R., 1998. Characteristics and origins of coal cleat: A review. International Journal of Coal Geology 35, 175–207. https://doi.org/10.1016/S0166-5162(97)00012-8
Lemmon, E.W., McLinden, M.O., Friend, D.G., 2020. Thermophysical Properties of Fluid Systems, in: NIST Standard Reference Database 69: NIST Chemistry WebBook. P.J. Linstrom and W.G. Mallard, National Institute of Standards and Technology, Gaithersburg MD, 20899.
Levine, J.R., 1996. Model study of the influence of matrix shrinkage on absolute permeability of coal bed reservoirs. Geological Society, London, Special Publications 109, 197–212. https://doi.org/10.1144/GSL.SP.1996.109.01.14
Liu, H.-H., Rutqvist, J., 2010. A new coal-permeability model: Internal swelling stress and fracture-matrix interaction. Transport in Porous Media 82, 157–171. https://doi.org/10.1007/s11242-009-9442-x
Liu, J., Chen, Z., Elsworth, D., Qu, H., Chen, D., 2011a. Interactions of multiple processes during CBM extraction: A critical review. International Journal of Coal Geology 87, 175–189. https://doi.org/10.1016/j.coal.2011.06.004
Liu, J., Wang, J., Chen, Z., Wang, S., Elsworth, D., Jiang, Y., 2011b. Impact of transition from local swelling to macro swelling on the evolution of coal permeability. International Journal of Coal Geology 88, 31–40. https://doi.org/10.1016/j.coal.2011.07.008
Liu, X., Sheng, J., Liu, J., Hu, Y., 2018. Evolution of coal permeability during gas injection—from initial to ultimate equilibrium. Energies 11, 2800. https://doi.org/10.3390/en11102800
Liu, Z., Cheng, Y., Wang, L., Wang, H., Jiang, J., Li, W., 2018. Analysis of coal permeability rebound and recovery during methane extraction: Implications for carbon dioxide storage capability assessment. Fuel 230, 298–307. https://doi.org/10.1016/j.fuel.2018.05.057
Lu, S., Cheng, Y., Li, W., 2016. Model development and analysis of the evolution of coal permeability under different boundary conditions. Journal of Natural Gas Science and Engineering 31, 129–138. https://doi.org/10.1016/j.jngse.2016.02.049
Mazumder, S., Karnik, A.A., Wolf, K.-H.A.A., 2006. Swelling of coal in response to CO2 sequestration for ECBM and its effect on fracture permeability. SPE Journal 11, 390–398. https://doi.org/10.2118/97754-PA
Moore, R.L., Loftin, D., Palmer, I., 2011. History matching and permeability increases of mature coalbed methane wells in San Juan basin, in: Asia Pacific Oil & Gas Conference and Exhibition. Jakarta, Indonesia, pp. 1–12.
Moore, T.A., 2012. Coalbed methane: A review. International Journal of Coal Geology 101, 36–81. https://doi.org/10.1016/j.coal.2012.05.011
Nazarova, L.A., Nazarov, L.A., Karchevsky, A.L., Vandamme, M., 2014. Estimating diffusion-capacity parameters of a coal bed using the gas pressure measured in a hole and the solution of an inverse problem. Journal of Applied and Industrial Mathematics 8, 267–273. https://doi.org/10.1134/S1990478914020136
Niu, Y., Mostaghimi, P., Shikhov, I., Chen, Z., Armstrong, R.T., 2018. Coal permeability: gas slippage linked to permeability rebound. Fuel 215, 844–852.
Ogunfunmi, T., 2007. Adaptive Nonlinear System Identification: The Volterra and Wiener Model Approaches, Signals and Communication Technology. Springer US.
Oudinot, A.Y., Koperna, G.J., Philip, Z.G., Liu, N., Heath, J.E., Wells, A., Young, G.B.C., Wilson, T., 2011. CO2 injection performance in the Fruitland Coal Fairway, San Juan basin: Results of a field pilot. SPE Journal 16, 864–879. https://doi.org/10.2118/127073-PA

1033 Palmer, I., Mansoori, J., 1998. How permeability depends on stress and pore pressure in coalbeds: A
1034 new model. SPE Reservoir Evaluation and Engineering 539–544.
1035 Pan, Z., Connell, L.D., 2012. Modelling permeability for coal reservoirs: A review of analytical models
1036 and testing data. International Journal of Coal Geology 92, 1–44.
1037 https://doi.org/10.1016/j.coal.2011.12.009
1038 Pan, Z.J., Connell, L.D., 2007. A theoretical model for gas adsorption-induced coal swelling.
1039 International Journal of Coal Geology 69, 243–252.
1040 Pekot, L.J., Reeves, S.R., 2002. Modeling the effects of matrix shrinkage and differential swelling on
1041 coalbed methane recovery and carbon sequestration.
1042 Peng, Y., Liu, J., Pan, Z., Connell, L.D., Chen, Z., Qu, H., 2017. Impact of coal matrix strains on the
1043 evolution of permeability. Fuel 189, 270–283. https://doi.org/10.1016/j.fuel.2016.10.086
1044 Peng, Y., Liu, J., Wei, M., Pan, Z., Connell, L.D., 2014a. Why coal permeability changes under free
1045 swellings: New insights. International Journal of Coal Geology 133, 35–46.
1046 https://doi.org/10.1016/j.coal.2014.08.011
1047 Peng, Y., Liu, J., Zhu, W., Pan, Z., Connell, L., 2014b. Benchmark assessment of coal permeability
1048 models on the accuracy of permeability prediction. Fuel 132, 194–203.
1049 https://doi.org/10.1016/j.fuel.2014.04.078
1050 Pijaudier-Cabot, G., Vermorel, R., Miqueu, C., Mendiboure, B., 2011. Revisiting poromechanics in the
1051 context of microporous materials. Comptes Rendus Mécanique 339, 770–778.
1052 https://doi.org/10.1016/j.crme.2011.09.003
1053 Pini, R., Ottiger, S., Burlini, L., Storti, G., Mazzotti, M., 2009. Role of adsorption and swelling on the
1054 dynamics of gas injection in coal. Journal of Geophysical Research 114, B04203.
1055 https://doi.org/10.1029/2008JB005961
1056 Qu, H., Liu, J., Pan, Z., Connell, L., 2014. Impact of matrix swelling area propagation on the evolution
1057 of coal permeability under coupled multiple processes. Journal of Natural Gas Science and
1058 Engineering 18, 451–466. https://doi.org/10.1016/j.jngse.2014.04.007
1059 Robertson, E., 2005. Modeling permeability in coal using sorption-induced strain data. Proceedings of
1060 SPE Annual Technical Conference and Exhibition 1–10. https://doi.org/10.2118/97068-MS
1061 Scott, M., Mazumder, S., Jiang, J., 2012. Permeability increase in Bowen basin coal as a result of
1062 matrix shrinkage during primary depletion, in: SPE Asia Pacific Oil and Gas Conference and
1063 Exhibition. Perth, Australia, pp. 1–21.
1064 Shi, J.Q., Durucan, S., 2004. Drawdown induced changes in permeability of coalbeds: A new
1065 interpretation of the reservoir response to primary recovery. Transport in Porous Media 56,
1066 1–16. https://doi.org/10.1023/B:TIPM.0000018398.19928.5a
1067 Somerton, W.H., Söylemezglu, I.M., Dudley, R.C., 1975. Effect of stress on permeability of coal.
1068 International Journal of Rock Mechanics and Mining Sciences & Geomechanics Abstracts 12,
1069 129–145. https://doi.org/10.1016/0148-9062(75)91244-9
1070 Vandamme, M., Brochard, L., Lecampion, B., Coussy, O., 2010. Adsorption and strain: The CO2-
1071 induced swelling of coal. Journal of the Mechanics and Physics of Solids 58, 1489–1505.
1072 https://doi.org/10.1016/j.jmps.2010.07.014
1073 Vandamme, M., Dangla, P., Nikoosokhan, S., Brochard, L., 2014. Modeling the poromechanical
1074 behavior of microporous and mesoporous solids: Application to coal, in: Nonlinear Elasticity
1075 and Hysteresis. Wiley-VCH Verlag GmbH & Co. KGaA, Weinheim, Germany, pp. 105–126.
1076 https://doi.org/10.1002/9783527665068.ch5
1077 Wang, L., Chen, Z., Wang, C., Elsworth, D., Liu, W., 2019. Reassessment of coal permeability evolution
1078 using steady-state flow methods: the role of flow regime transition. International Journal of
1079 Coal Geology 211, 103210.
1080 Wang, S., Elsworth, D., Liu, J., 2011. Permeability evolution in fractured coal: The roles of fracture
1081 geometry and water-content. International Journal of Coal Geology 87, 13–25.
1082 https://doi.org/10.1016/j.coal.2011.04.009

Wei, M., Liu, J., Elsworth, D., Li, S., Zhou, F., 2019a. Influence of gas adsorption induced non-uniform deformation on the evolution of coal permeability. International Journal of Rock Mechanics and Mining Sciences 114, 71–78. https://doi.org/10.1016/j.ijrmms.2018.12.021

Wei, M., Liu, J., Shi, R., Elsworth, D., Liu, Z., 2019b. Long-term evolution of coal permeability under effective stresses gap between matrix and fracture during CO2 injection. Transport in Porous Media 130, 969–983.

Wold, M.B., Connell, L.D., Choi, S.K., 2008. The role of spatial variability in coal seam parameters on gas outburst behaviour during coal mining. International Journal of Coal Geology 75, 1–14. https://doi.org/10.1016/j.coal.2008.01.006

Wu, Y., Liu, J., Chen, Z., Elsworth, D., Pone, D., 2011. A dual poroelastic model for CO2-enhanced coalbed methane recovery. International Journal of Coal Geology 86, 177–189. https://doi.org/10.1016/j.coal.2011.01.004

Wu, Y., Liu, J.S., Elsworth, D., Chen, Z.W., Connell, L., Pan, Z.J., 2010. Dual poroelastic response of a coal seam to CO2 injection. International Journal of Greenhouse Gas Control 4, 668–678. https://doi.org/10.1016/j.ijggc.2010.02.004

Zang, J., Wang, K., 2017. Gas sorption-induced coal swelling kinetics and its effects on coal permeability evolution: Model development and analysis. Fuel 189, 164–177. https://doi.org/10.1016/j.fuel.2016.10.092

Zhao, W., Cheng, Y., Pan, Z., Wang, K., Liu, S., 2019. Gas diffusion in coal particles: A review of mathematical models and their applications. Fuel 252, 77–100. https://doi.org/10.1016/j.fuel.2019.04.065